THE MANGANESE SILICATE ROCKS OF THE EARLY PROTEROZOIC VITTINKI GROUP, SOUTHWESTERN FINLAND: METAMORPHIC GRADE AND GENETIC INTERPRETATIONS

FRANCO MANCINI[§]

Geological Survey of Japan, 1-1-3 Higashi, Tsukuba 305, Japan

REIJO ALVIOLA

Geological Survey of Finland, P.O. Box 96, FIN-02151 Espoo, Finland

BRIAN MARSHALL

Applied Geology Unit, University of Technology – Sydney, P.O. Box 123, Sydney, Australia

HISAO SATOH

Geological Survey of Japan, 1-1-3 Higashi, Tsukuba 305, Japan

HEIKKI PAPUNEN

Department of Mineralogy and Geology, Turku University, FIN-20014 Turku, Finland

ABSTRACT

The manganese silicate rocks of the Vittinki Group, in southwestern Finland, are interbedded with metachert, and are associated with amphibolitic metavolcanic rocks that have been metamorphosed to a temperature of up to $740 \pm 30°C$ and a pressure of between 4 and 5 kbar. They are interpreted as the metamorphosed equivalent of "distal" submarine hydrothermal deposits of Mn–Fe-bearing interlayered silica-rich and carbonate-rich sediments. The metachert comprises a dominant Fe-rich silicate facies (with quartz, fayalite, ferrosilite, pyrrhotite, magnetite, annite, grunerite) and subordinate calc-silicate intercalations (with calcite, dolomite, siderite, diopside, tremolite, fayalite, quartz), consistent with $X(CO_2)$ exhibiting abrupt lithologically controlled changes during peak metamorphism. The manganese silicate lenses consist of rhodonite, pyroxmangite, manganocummingtonite, manganogrunerite, tephroite, rhodochrosite, calcite, pyrrhotite and magnetite. The metamorphic assemblages reflect low and unbuffered $X(CO_2)$ values and intermediate- to low-$f(O_2)$ conditions. Consistent with an origin by polysomatic transformation from a "protorhodonite" precursor, the rhodonite contains abundant lamellae of pyroxmangite and clinopyroxene defects that persisted metastably at peak conditions of metamorphism. The synmetamorphic quartz – amphibole $\pm$ braunite veins originated from oxidized fluids. The oxygen isotope exchange thermometer between quartz and manganoan cummingtonite yields equilibration temperatures of $640 \pm 30°C$.

Keywords: metamorphism, manganese silicate rocks, pyroxenoids, manganocummingtonite, oxygen-isotope ratios, chain-periodicity defects, Vittinki Group, Finland.

SOMMAIRE

Les roches à silicates de manganèse du Groupe de Vittinki, dans le sud-est de la Finlande, sont interlitées avec des métacherts, et associées avec des roches métavolcaniques, maintenant des amphibolites, l'ensemble ayant été métamorphisé à une température atteignant environ $740 \pm 30°C$ à une pression d'environ 4–5 kbar. Cet ensemble serait l'équivalent métamorphisé de roches sous-marines exhalatives distales, composées d'horizons de sédiments siliceux riches en Mn et Fe et d'horizons carbonatés. Les métacherts contiennent un faciès à dominance de silicates de fer (avec quartz, fayalite, ferrosilite, pyrrhotite, magnétite, annite, grunerite), avec intercalations subordonnées de calc-silicates (avec calcite, dolomite, sidérite, diopside, trémolite, fayalite, quartz),

[§] *Present address*: Department of Earth and Planetary Sciences, American Museum of Natural History, Central Park West at 79th Street, New York, N.Y. 10024-5192, U.S.A.
E-mail address: mancini@amnh.org

ce qui fait penser que $X(CO_2)$ variait abruptement selon les assemblages développés lors de la recristallisation métamorphique. Les lentilles de silicates de manganèse contiennent rhodonite, pyroxmangite, manganocummingtonite, manganogrunerite, tephroïte, rhodochrosite, calcite, pyrrhotite et magnétite. Les assemblages métamorphiques témoignent de faibles valeurs de $X(CO_2)$ non régies par les assemblages et une fugacité d'oxygène intermédiaire à faible. Conforme à une origine par transformation polysomatique à partir d'un précurseur "protorhodonitique", la rhodonite contient d'abondantes lamelles de pyroxmangite et des défauts de clinopyroxène qui ont survécu de façon métastable aux conditions du paroxysme métamorphique. Les veines synmétamorphiques contenant quartz – amphibole ± braunite se sont formées à partir d'une phase fluide oxygénée. Le géothermomètre fondé sur l'équilibre d'échange des isotopes d'oxygène dans le quartz et la cummingtonite manganifère indiquent une température de $640 \pm 30°C$.

(Traduit par la Rédaction)

Mots-clés: métamorphisme, roches à silicates de manganèse, pyroxénoïdes, manganocummingtonite, rapports des isotopes d'oxygène, défauts de périodicité des chaînes, Groupe de Vittinki, Finlande.
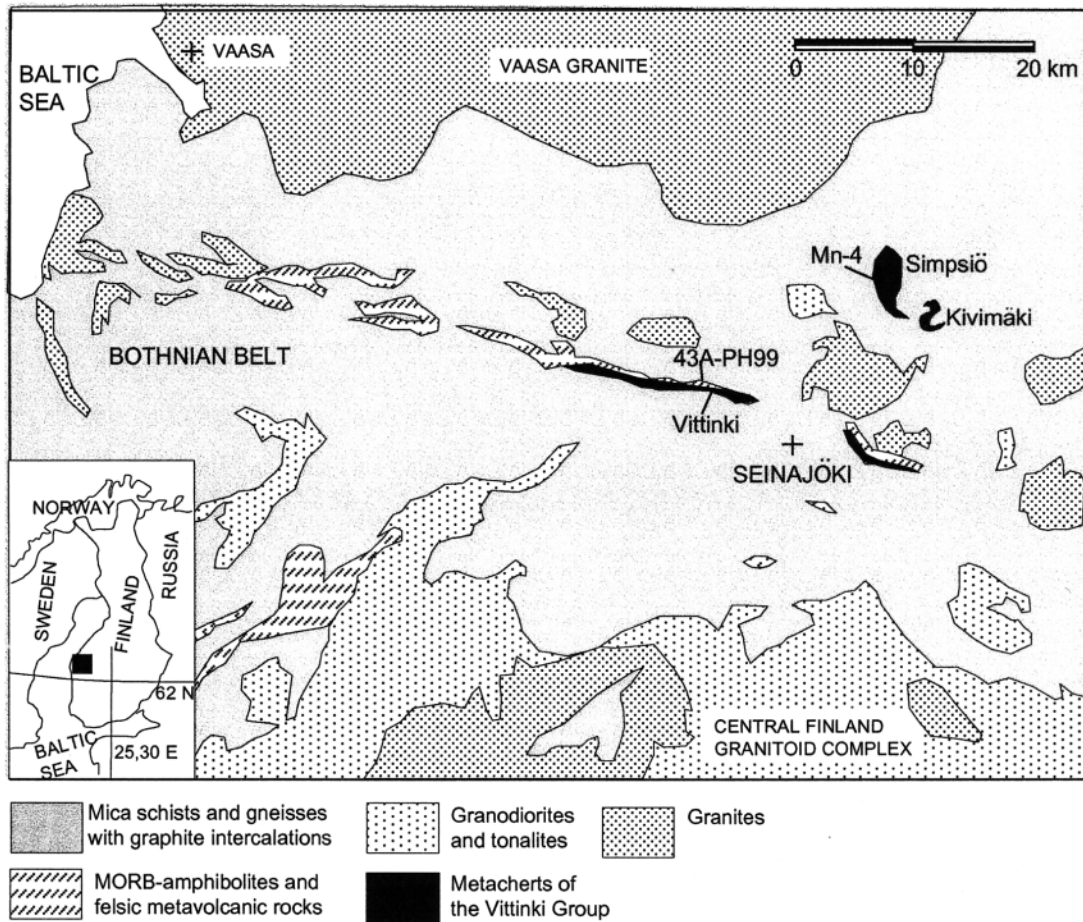

FIG. 1. Simplified geological map showing the major units of the Bothnian Belt and the location of the Vittinki Group. Note that samples Mn–4 (manganese silicate rock at Simpsiö) and 43A–PH–99 (country-rock amphibolite at Vittinki), outside the outcrop maps (Fig. 2), also are indicated.
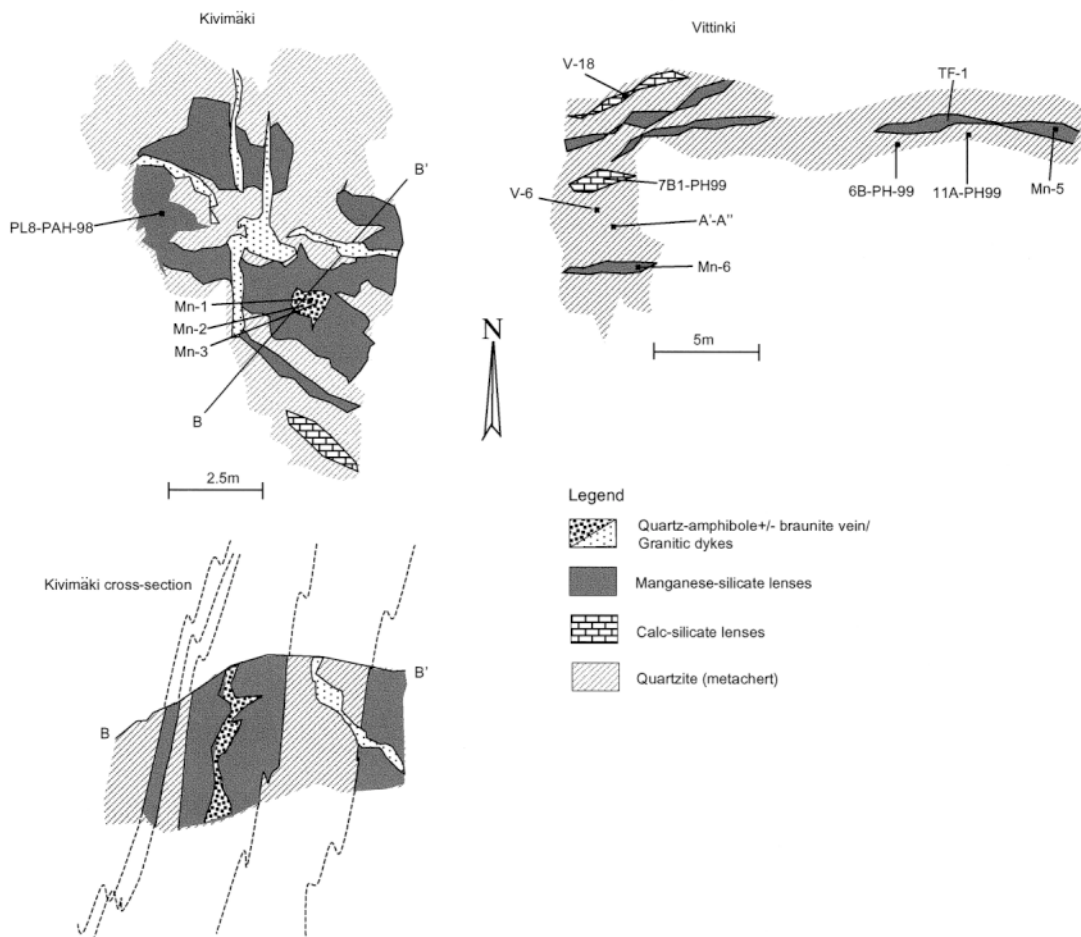
FIG. 2. Schematic outcrop maps at Kivimäki and Vittinki, showing the principal rock-types forming the Vittinki Group and the location of the samples for this study.

INTRODUCTION

At Vittinki and near Kivimäki, ~20 km from the town of Seinäjoki, in southwestern Finland (Figs. 1, 2), scattered outcrops of the Vittinki Group consist of bands of manganese silicate rocks interbedded with quartzose rocks and subordinate calc-silicate lenses (*e.g.,* Mäkitie & Lahti 1991). Minor concentrations of rhodonite and pyroxmangite within quartzite also were found nearby at Simpsiö (Hietanen 1938). The sequence is part of an association of MORB-type metavolcanic rocks, metapelitic schists and various gneissic rocks that belongs to the 1.88–1.90-Ga-old Proterozoic Svecofennian domain in southwestern Finland (*e.g.,* Gaál & Gorbatchev 1987). The manganese silicate rocks are poorly exposed and have received little attention, despite the fact that

Saxén (1925) and Hietanen (1938) noted the presence of rhodonite, and Törnroos (1982) reported the presence of alabandite, a relatively rare mineral.

In the present article, we describe the metamorphic assemblages of the manganese silicate rocks and their host rocks from the point of view of the textural relationships and mineral chemistry of the constituent phases. As part of the textural analysis, the microstructures in rhodonite, the principal mineral phase, are characterized by transmission electron microscopy (TEM). The formation of $Mn–Fe^{2+}$ silicates, *e.g.,* tephroite and pyroxenoids, requires a restricted bulk-rock composition (*i.e.,* intermediate SiO_2 content and a high Mn:Fe ratio) and a metamorphic fluid characterized by low activities of H_2O, CO_2 and O_2 (Peters *et al.* 1978, Abs-Wurmbach *et al.* 1983, Ashley 1989, Lucchetti 1991,

Dasgupta *et al.* 1993). The petrological and mineralogical data, coupled with relevant experimental results in the Mn-rich system (Peters *et al.* 1973, Candia *et al.* 1975, Huebner 1986), are used to constrain conditions of metamorphism. Moreover, data on bulk compositions are interpreted in terms of the premetamorphic character and geological setting of the metasedimentary units, thereby contributing to the metallogenic record of this sector of the Baltic Shield.

Geological background and occurrence of the Vittinki Group

The Bothnian Belt of the Svecofennides hosts the Vittinki Group (Fig. 1); it is part of a large subduction-zone system that developed 2.1–1.89 Ga ago on the southern margin of the Karelian continent, and comprises a range of intrusive bodies (granites, tonalites and ultramafic complexes) and metamorphosed supracrustal sequences containing schists and gneisses, metacherts and metavolcanic rocks (*e.g.,* Gaál & Gorbatchev 1987, Niironen 1997, and references therein). Vaarma & Kähkönen (1994) indicated that the metavolcanic rocks range from MORB-type to predominantly arc-type basalts and andesites. Regional Svecofennian metamorphism, which culminated at 1.89 Ga with the closure of the Bothnian basin, consisted of a protracted high-temperature event that was accompanied by a polyphase (D_1–D_3) deformation before temperature decay over a near-isobaric cooling-path (Kilpeläinen 1998). In some parts of the Bothnian Belt, conditions consistent with the transition between the upper-amphibolite and lower-granulite facies (*i.e.,* T in the range 700–750°C and 5 ± 1 kbar) were determined (Korsman *et al.* 1984, Niironen 1997). However, in the region encompassing the Vittinki Group, peak conditions are generally masked owing to overprinting by lower amphibolite- or even greenshist-facies retrograde assemblages (Mäkitie & Lahti 1991).

The Vittinki Group, which is of unknown thickness, consists principally of banded quartzite (metachert), subordinate calc-silicate intercalations containing siderite, dolomite, calcite, diopside, forsterite, fayalite, magnetite, tremolite and quartz, and uncommon manganese-silicate-enriched lenses (Fig. 2). The centimeter-thick banding in the metachert is defined by variable
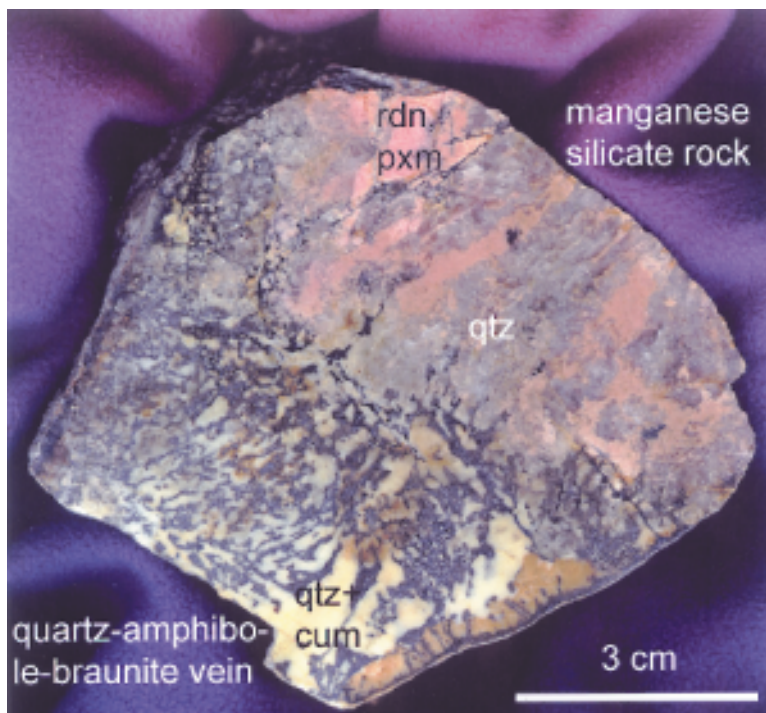

FIG. 3.   Hand-sample of the manganese silicate rocks and of the quartz – amphibole ± braunite vein adjacent the contact. Note the discordant contact and the black manganese oxyhydroxide in the vein, formed during the incipient weathering of braunite and other manganese-bearing silicates. Mineral abbreviations: rdn: rhodonite, pxm: pyroxmangite, qtz: quartz, cum: manganocummingtonite.

concentrations of minor phases such as iron oxide (magnetite), iron sulfides (pyrite, pyrrhotite, mackinawite and troilite), iron silicates (ferrosilite, fayalite and grunerite), graphite and siderite. The apparently conformable manganese silicate lenses are 0.2 to 3.5 m thick, have a 3–5-mm surficial coating of supergene manganese oxyhydroxide, and are massive or layered. In the latter case, the 0.5–2-cm-thick layering consists of pink-red rhodonite-rich bands alternating with translucent quartz-rich bands (Fig. 3). The banding, which conforms with the S1 schistosity in the country rocks, could be entirely secondary (*i.e.,* metamorphic), or involve transposition of primary layering. In some places, the manganese silicate lenses contain brownish green nodules and pods (maximum diameter 1.5 m) dominated by tephroite. A sequence of metavolcanic units (100–200 m thick) with intercalations of migmatitic gneiss and graphite schist are juxtaposed to the Vittinki Group metachert (Hietanen 1938, Mäkitie & Lahti 1991). Because contacts with the metachert are not exposed, it is unclear whether the relationships reflect original stratigraphic succession or tectonic reworking.

The manganese-rich lenses host two generations of veins. The older set consists of synmetamorphic quartz – amphibole ± braunite veins that have a pervasive lineation and subvertical dip (Fig. 2). They are discordant to banding (Fig. 3), having been emplaced up the hinge surface of F_2 folds (*cf.* Kilpeläinen 1998). The younger set consists of lenticular quartz veins that contain medium- to coarse-grained quartz – albite – spessartine assemblages in the thicker portions.

MINERAL ASSOCIATIONS IN THE HOST METACHERT

The metachert consists predominantly of a microcrystalline quartz groundmass (grain size 0.1–0.3 mm) hosting various accessory phases. The following associations are distinguished: i) quartz – fayalite – pyrrhotite – magnetite ± pyrite ± graphite; ii) quartz – ferrosilite – magnetite – grunerite – annite ± fayalite; and iii) quartz – magnetite – pyrrhotite – pyrite ± graphite.

In association i) (*e.g.,* sample A–A') fayalite is pleochroic from pale brown to yellowish brown, forms aggregates of subhedral, nearly equidimensional grains, up to 1 mm in diameter, and is nearly the pure end-member in composition (*i.e.,* $Fa_{0.95}Fo_{0.02}Te_{0.03}$; see Table 1). Where fayalite coexists with minor sulfides and magnetite, the quartz – fayalite – pyrrhotite ± pyrite ± magnetite aggregates (up to 0.7 cm thick) impart a lenticular layering to the rock. Fayalite grains in the aggregates have smooth "clean" boundaries against quartz, which generally occurs as trains of smaller grains separating the mineral from the pyrrhotite. The textures are consistent with olivine forming by a possible reaction between quartz (chert) and original sedimentary carbonates (the latter being fully consumed) without participation of the sulfide (*e.g.,* Bonnichsen 1969). Cross-cutting veinlets of now-undulose quartz could reflect synkinematic retrograde mobilization of SiO_2.

In association ii) (*e.g.,* sample 6B–PH99), ferrosilite ($Fs_{0.73}En_{0.121}Rdn_{0.1}$: Table 1) usually forms a medium-grained (1–2 mm) polygonal aggregate together with quartz and minor magnetite. The ferrosilite is pleochroic from dark brown to yellowish brown, and crystallized directly as orthopyroxene, rather than inverting from pigeonite. Where coexisting with fayalite, it is richer in Fe. Sporadically, the ferrosilite aggregates encompass porphyroblastic masses of pyrrhotite and, less commonly, pyrite. The orthopyroxene also occurs as large grains, up to 1 cm across, that appear to have a preferred orientation parallel to the layering and that poikiloblastically enclose roundish quartz, microcrystalline magnetite and quartz. Some of the original poikiloblasts have recrystallized to form subgrain aggregates. Accessory grunerite is mainly present as submicroscopic needles rimming orthopyroxene grains. This texture, together with the inclusions of magnetite, suggests oxidation during retrograde hydration according to the replacement reaction:

$$8\ FeSiO_3 + H_2O + 1/6\ O_2$$
$$= Fe_7Si_8O_{22}(OH)_2 + 1/3\ Fe_3O_4 \qquad (1)$$
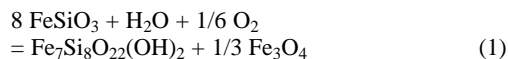
Less commonly, needles of grunerite (0.05 mm across) occur in stellate aggregates around euhedral magnetite, possibly the result of the prograde reduction reaction:

$$7\ Fe_3O_4 + 24\ SiO_2 + 3\ H_2O$$
$$= 3\ Fe_7Si_8O_{22}(OH)_2 + 7/2\ O_2 \qquad (2)$$

TABLE 1. REPRESENTATIVE COMPOSITIONS OF MINERALS IN THE QUARTZITE (METACHERT) OF THE VITTINKI GROUP, SOUTHWESTERN FINLAND

Locality Sample	Vittinki 6B-PH 99			Vittinki A-A'		
Mineral	fs	fs	fa	fa	fa	fa
SiO_2(wt%)	47.42	48.19	30.80	30.73	30.65	30.68
TiO_2	0.03	0.03	<d.l.	<d.l.	<d.l.	<d.l.
Al_2O_3	0.14	0.11	<d.l.	<d.l.	<d.l.	<d.l.
Cr_2O_3	0.03	0.05	0.18	<d.l.	0.06	<d.l.
FeO_{tot}	41.50	41.36	68.86	68.31	68.86	68.52
MnO	5.62	5.49	1.45	1.07	1.18	0.84
MgO	3.83	3.90	0.59	0.66	0.55	0.38
CaO	0.72	0.72	<d.l.*	<d.l.	<d.l.	<d.l.
Total	99.30	99.87	101.8	100.8	101.3	100.4
No. Ox.	3	3	4	4	4	4
Si(atoms)	1.00	1.01	1.01	1.02	1.01	1.02
Ti	0.00	0.00	0.00	0.00	0.00	0.00
Al	0.00	0.00	0.00	0.00	0.00	0.00
Cr	0.00	0.00	0.00	0.00	0.00	0.00
Fe^{2+}	0.74	0.73	1.89	1.89	1.90	1.91
Mn	0.10	0.09	0.04	0.03	0.03	0.02
Mg	0.12	0.12	0.03	0.03	0.03	0.02
Ca	0.01	0.01	0.00	0.00	0.00	0.00
$Mg/(Mg+Fe^{2+})$	0.14	0.14	0.01	0.01	0.01	0.01

Mineral abbreviations: fs=ferrosilite; fa=fayalite.
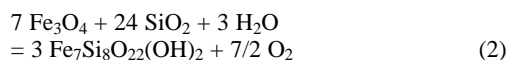*Detection limits (d.l.): Na_2O, K_2O, SiO_2, CaO, MgO, Cr_2O_3, Al_2O_3=0.01wt%; FeO=0.03wt%; MnO=0.02wt%; F=0.1wt%.
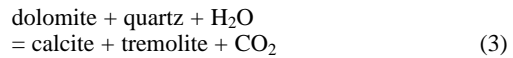
In association iii), which lacks Fe-silicates, microme-
ter-size grains of the unweathered sulfides, pyrrhotite
and pyrite (the former altering to mackinawite), together
with graphite flakes, form irregular stringers and veins,
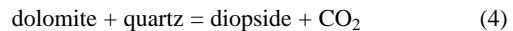up to 1 cm thick, in a quartz groundmass. The relatively

larger grains of sphalerite, a rare constituent of the
stringers, contain submicroscopic blebs of chalcopyrite.

The subordinate calc-silicate intercalations are sepa-
rated from the quartzite by a 1–2 cm transitional zone
consisting of prismatic diopside and tremolite oriented
normal to the contacts. Three distinct mineral associa-
tions are recognized in the calc-silicate lenses: i) diop-
side – tremolite ± dolomite ± quartz; ii) calcite –
dolomite; and iii) fayalite – calcite – siderite – dolomite
± magnetite.

In association i) (*e.g.,* sample V–18), diopside occu-
pies 80–90 vol.%, and forms a granoblastic aggregate
of ragged grains, 0.2–1.0 mm across. Dolomite and
quartz are found as irregular aggregates of anhedral
grains either overgrown by diopside or transected by
tremolite nematoblasts. This textural evidence is con-
sistent with the prograde sequence for the following
reactions, after Spear (1993), among others:

$$\text{dolomite} + \text{quartz} + H_2O$$
$$= \text{calcite} + \text{tremolite} + CO_2 \qquad (3)$$

and

$$\text{dolomite} + \text{quartz} = \text{diopside} + CO_2 \qquad (4)$$

which intersect at an invariant point in T–$X(CO_2)$ space
[*i.e.,* at $X(CO_2) = 0.88$ at T = 580°C and P = 5 kbar:
Spear 1993].

In association ii), dolomite and calcite have recrys-
tallized into a polygonal aggregate with a grain size in
the order of 1–2 mm, whereas in association iii) (*e.g.,*

TABLE 2. REPRESENTATIVE COMPOSITIONS OF MINERALS
IN THE CALC-SILICATE LENSES OF THE VITTINKI GROUP,
SOUTHWESTERN FINLAND

Locality	Vittinki						
Sample	7B1-PH99						
Mineral	fa	fa	fa	cal	cal	sd	dol
SiO₂(wt%)	34.19	34.19	34.22	0.03	<d.l.*	<d.l.	<d.l.
Al₂O₃	<d.l.	<d.l.	<d.l.	<d.l.	0.02	<d.l.	<d.l.
TiO₂	<d.l.	<d.l.	<d.l.	0.03	<d.l.	<d.l.	<d.l.
FeO_tot	42.36	41.78	42.06	0.85	2.17	37.60	4.71
MgO	21.64	21.40	21.66	0.62	3.61	<d.l.	16.37
MnO	2.19	1.97	2.12	1.10	1.15	<d.l.	1.08
Cr₂O₃	<d.l.	<d.l.	<d.l.	<d.l.	<d.l.	0.02	<d.l.
CaO	<d.l.	0.16	0.14	53.18	52.39	0.123	28.96
Na₂O	<d.l.	<d.l.	0.02	<d.l.	0.03	<d.l.	<d.l.
K₂O	<d.l.	<d.l.	<d.l.	<d.l.	<d.l.	<d.l.	<d.l.
Total	100.4	99.51	100.2	55.83	59.38	37.79	51.18
No. Ox.	4	4	4	12	12	12	12
Si(atoms)	0.99	1.00	0.99	0.00	0.00	0.00	0.00
Al	0.00	0.00	0.00	0.00	0.00	0.00	0.00
Ti	0.00	0.00	0.00	0.00	0.00	0.00	0.00
Fe²⁺	1.03	1.02	1.02	0.05	0.11	3.97	0.26
Mg	0.94	0.93	0.94	0.06	0.33	0.00	1.62
Mn	0.05	0.05	0.05	0.06	0.06	0.00	0.06
Cr	0.00	0.00	0.00	0.00	0.00	0.00	0.00
Ca	0.00	0.00	0.00	3.82	3.49	0.02	2.06
Na	0.00	0.00	0.00	0.00	0.00	0.00	0.00
K	0.00	0.00	0.00	0.00	0.00	0.00	0.00
Mg/(Mg+Fe²⁺)	0.47	0.47	0.47	0.37	0.75	0.00	0.86

Mineral abbreviations: fa=fayalite cal=calcite, sd=siderite, dol=dolomite.
*Detection limits as in Table 1

TABLE 3. REPRESENTATIVE COMPOSITIONS OF MINERALS IN THE MANGANESE SILICATE ROCKS OF THE VITTINKI GROUP,
SOUTHWESTERN FINLAND

Locality	Simpsiö					Vittinki				Vittinki		Simpsiö				Vittinki	
Sample	Mn-4					Mn-6				Mn-5		Mn-4				TF-1	
Mineral	rdn	pxm	rdn	cal	pxm	rds	pxm	pxm	mgt	sps	rdn	cum(p)*		gru		tep	rdn
SiO₂(wt%)	46.68	45.98	46.08	<d.l.	46.19	0.02	45.94	46.16	0.16	36.26	45.04	52.13	52.17	50.88	51.49	31.61	39.75
TiO₂	<d.l.**	<d.l.	0.03	0.03	<d.l.	<d.l.	<d.l.	0.02	0.12	<d.l.	<d.l.	<d.l.	<d.l.	<d.l.	<d.l.	<d.l.	<d.l.
Al₂O₃	<d.l.	<d.l.	<d.l.	<d.l.	<d.l.	<d.l.	<d.l.	<d.l.	0.18	20.65	<d.l.	<d.l.	<d.l.	<d.l.	<d.l.	<d.l.	<d.l.
Cr₂O₃	<d.l.	<d.l.	<d.l.	<d.l.	<d.l.	<d.l.	<d.l.	<d.l.	<d.l.	<d.l.	<d.l.	<d.l.	<d.l.	<d.l.	<d.l.	<d.l.	<d.l.
FeO_tot	8.93	18.73	16.04	2.22	19.47	1.28	18.53	18.43	0.00	0.38	0.52	19.77	19.87	24.72	25.37	0.59	0.19
Fe₂O₃	0.00	0.00	0.00	0.00	0.00	0.00	0.00	0.00	97.82	0.00	0.00	0.00	0.00	0.00	0.00	0.00	0.00
MnO	35.26	31.03	29.70	13.73	29.55	48.30	28.35	28.10	1.27	39.29	50.23	10.68	10.99	10.98	10.71	62.75	54.83
MgO	2.80	1.98	1.46	0.57	2.16	0.26	2.40	2.96	<d.l.	1.29	0.49	12.12	12.13	8.87	8.85	3.32	2.08
CaO	5.34	2.11	5.01	40.86	2.41	3.35	3.45	3.08	0.05	0.67	1.76	1.02	1.06	0.78	0.91	0.10	1.87
Na₂O	<d.l.	<d.l.	<d.l.	0.03	0.04	0.05	<d.l.	0.02	<d.l.	<d.l.	<d.l.	0.07	0.07	0.08	0.04	<d.l.	<d.l.
K₂O	<d.l.	<d.l.	<d.l.	<d.l.	<d.l.	<d.l.	<d.l.	<d.l.	<d.l.	<d.l.	<d.l.	<d.l.	<d.l.	<d.l.	<d.l.	<d.l.	<d.l.
Total	99.02	99.84	98.33	57.44	99.82	53.25	98.68	98.78	99.62	98.54	98.05	95.78	96.29	96.29	97.36	98.43	98.72
No. Ox.	6	6	6	9	6	9	6	6	4	12	6	23	23	23	23	4	6
Si(atoms)	1.99	1.98	2.00	0.00	1.99	0.00	1.99	1.99	0.00	2.99	1.99	8.04	8.02	8.02	8.03	1.04	1.82
Ti	0.00	0.00	0.00	0.00	0.00	0.00	0.00	0.00	0.00	0.00	0.00	0.00	0.00	0.00	0.00	0.00	0.00
Al	0.00	0.00	0.00	0.00	0.00	0.00	0.00	0.00	0.01	2.01	0.00	0.00	0.00	0.00	0.00	0.00	0.00
Fe²⁺	0.32	0.68	0.58	0.10	0.70	0.07	0.67	0.66	0.00	0.02	0.02	2.55	2.56	3.26	3.31	0.02	0.00
Fe³⁺	0.00	0.00	0.00	0.00	0.00	0.00	0.00	0.00	2.67	0.00	0.00	0.00	0.00	0.00	0.00	0.00	0.00
Mn	1.27	1.13	1.09	0.60	1.08	2.67	1.04	1.03	0.04	2.75	1.88	1.40	1.43	1.47	1.42	1.74	2.12
Mg	0.18	0.13	0.09	0.04	0.14	0.02	0.15	0.19	0.00	0.16	0.03	2.79	2.78	2.08	2.06	0.16	0.14
Ca	0.24	0.10	0.23	2.26	0.11	0.23	0.16	0.14	0.00	0.06	0.08	0.17	0.17	0.13	0.15	0.00	0.10
Na	0.00	0.00	0.00	0.00	0.00	0.01	0.00	0.00	0.00	0.00	0.00	0.02	0.02	0.02	0.01	0.00	0.00
K	0.00	0.00	0.00	0.00	0.00	0.00	0.00	0.00	0.00	0.00	0.00	0.00	0.00	0.00	0.00	0.00	0.00
Mn/Mn+Mg)	0.87	0.89	0.92	0.93	0.88	1.00	0.87	0.84	0.00	0.94	0.98	0.33	0.34	0.41	0.41	0.91	0.93
Mg/(Mg+Mn+Fe²⁺)	0.10	0.07	0.05	0.2	0.07	0.00	0.08	0.10	0.00	0.05	0.01	0.41	0.41	0.31	0.30	0.08	0.06
Mg/(Mg+Fe²⁺)	0.36	0.16	0.13	0.28	0.16	0.22	0.18	0.22	0.00	0.11	0.6	0.52	0.52	0.39	0.38	0.88	1.00

Mineral abbreviations: rdn: rhodonite, pxm: pyroxmangite, cal: calcite, rds: rhodochrosite, sps: spessartine, cum: manganocummingtonite, gru: manganogrunerite,
mgt: magnetite, tep: tephroite.   *(p): porphyroblastic.   ** Detection limits as in Table 1.

sample 7B1–PH99), fayalite and coexisting siderite, calcite and dolomite (Table 2) form a finer-grained polygonal granoblastic aggregate (grain size 0.1–1 mm) with dispersed magnetite at triple points. The subhedral roundish fayalite ($Fa_{0.51}Fo_{0.46}Te_{0.03}$: Table 2) makes up 30–50 vol.% of the rock. The lack of quartz in associations ii) and iii), and the persistence of carbonates at high grade, are in this case ascribed to the limited amount of pre-metamorphic quartz and its rapid consumption by reactions with early carbonates.

<div style="text-align:center">

MINERAL ASSOCIATIONS
IN THE MANGANESE SILICATE LENSES

</div>

Three mineral associations are recognized: i) rhodonite – pyroxmangite – manganocummingtonite or manganogrunerite ± magnetite; ii) rhodonite – rhodochrosite ± pyrrhotite ± magnetite ± graphite; and iii) tephroite – rhodonite ± rhodochrosite ± quartz ± magnetite. For simplicity, cummingtonite is here used for all Mn-rich amphiboles of the cummingtonite–grunerite

and manganocummingtonite–manganogrunerite series, even though some have Mg/(Mg + Fe) less than 0.5 and are grunerite or manganogrunerite in terms of IMA nomenclature.

In associations i) (*e.g.,* sample Mn–4 and Mn–6) and ii) (*e.g.,* sample Mn–5), rhodonite and pyroxmangite occur as subhedral prismatic grains (0.2–2 mm in size), or as poikiloblasts (up to 1.5 cm across) enclosing rare partially chloritized grains of spessartine. Submicroscopic grains of magnetite and pyrrhotite occupy triple-point junctions and are less commonly present as inclusions. In the rhodonite, $FeSiO_3$ content ranges from ~1 up to 34 mole%, whereas the $CaSiO_3$ content ranges between 14 and 2 mole % (Table 3). Many rhodonite grains contain micrometric (001) and (100) lamellae (see below), whereas others host patchy intergrowths of pyroxmangite (Fig. 4a). Separate grains of pyroxmangite were distinguished from rhodonite by their relatively smaller $2V\gamma$ ($2V\gamma_{rdn}$ in the range 62–89°, $2V\gamma_{pxm}$ in the range 30–48°), by the absence of fine lamellae, and by its bulk composition (Fig. 5a). Pyroxmangite has
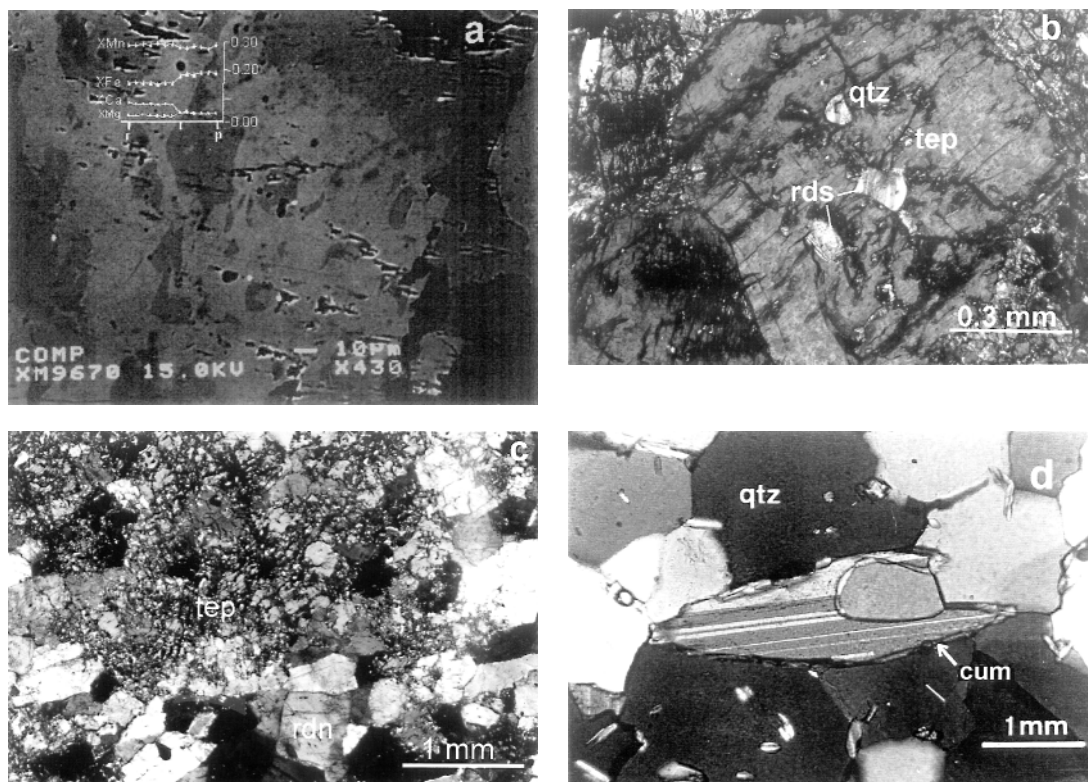

FIG. 4. Microtextures of the manganese silicate rocks. a) Back-scattered electron image of rhodonite containing patchy intergrowths of pyroxmangite (darker) (sample Mn–6); the inset diagram shows the compositional variation along the r–p profile (*i.e.*, the horizontal axis). b) Tephroite (tep) porphyroblast with relict rhodochrosite (rds) and quartz (qtz) inclusions (crossed nicols) (sample TF–1). c) Rhodonite (rdn) replacing tephroite (tep) (crossed nicols) (sample TF–1). d) Quartz (qtz) – cummingtonite (cum) assemblage in the synmetamorphic veins (crossed nicols).
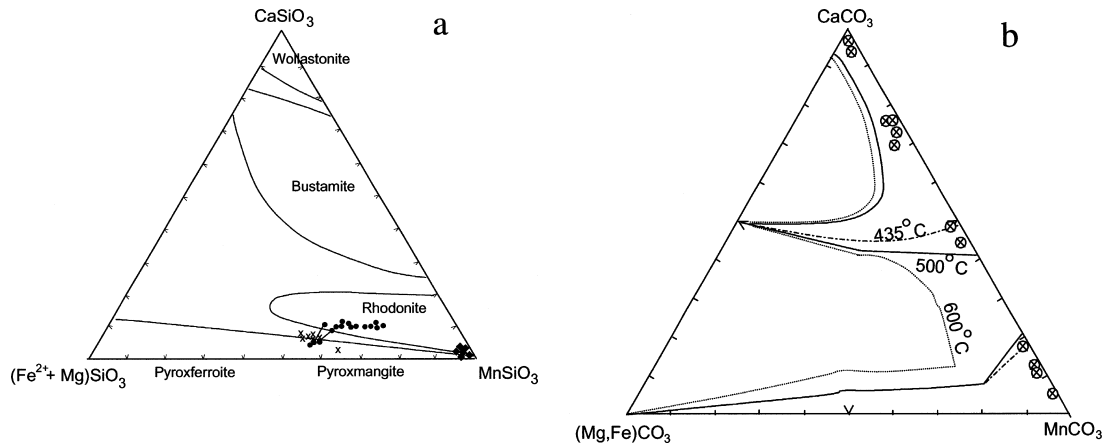
FIG. 5.   a) Plot of rhodonite and pyroxmangite compositions in the diagram $CaSiO_3$ – $MnSiO_3$ – $(Fe + Mg)SiO_3$. Symbols: Mn–4: crosses, Mn–5: diamonds, Mn–6: filled circles. Coexisting minerals are connected by tielines. Fields for various pyroxenoids according to Brown *et al.* (1980). b) Composition of carbonates in samples Mn–4 – Mn–6 plotted onto the $CaCO_3$ – $MnCO_3$ – $(FeCO_3 + MgCO_3)$ diagram. The curves indicate the solvus at various temperatures (after Goldsmith & Graf 1957).

a $FeSiO_3$ content up to 38 mole %, whereas $MgSiO_3$ is generally below 8 mole %. In the most iron-rich samples (*e.g.,* PL8–PAH98), pinkish pyroxmangite [Mn/(Mn + Fe) in the range 0.50–0.53] coexists with orange-colored pyroxferroite [Mn/(Mn + Fe) in the range 0.47–0.49] (Mancini *et al.*, in prep.). Magnetite in the assemblages contains negligible amounts of Mn, Al, Ti and Mg. The spessartine is almost pure, having a negligible Fe^{3+} content (Table 3) which, according to Hsu (1968) is consistent with formation at low $f(O_2)$, below the hematite–magnetite buffer, possibly from the reaction

$$\text{quartz + pennantite = spessartine} + H_2O \qquad (5)$$
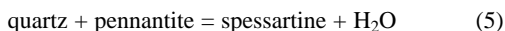
at T ≈ 400°C.

Cummingtonite is invariably a product of retrograde replacement. In association i), cummingtonite ($2V\gamma$ in the range 76–80°, $c \wedge \gamma$ in the range 9–13°) is present as porphyroblastic grains (2–3 mm across) overgrowing rhodonite grains, and as finer needles replacing the rhodonite along its cleavages. The Mn content ranges from 1.21 to 1.52 atoms per formula unit (*apfu*). The porphyroblasts have Mg/(Mg + Mn + Fe) in the range 0.39–0.43 (Table 3), whereas the nematoblastic cummingtonite has Mg/(Mg + Mn + Fe) in the range 0.29–0.38, this being consistent with a lower temperature of crystallization (*e.g.,* Huebner 1986). Because the Mg and Fe contents of cummingtonite exceed those of the replaced rhodonite, some degree of metasomatism during hydration is probable (see later discussion).

Tephroite comprises over 60–70 vol.% of association iii) (*e.g.,* sample TF–1), is weakly pleochroic from greenish gray to brownish green, and has $2V\gamma$ in the range 64–70°. The coexisting pyroxenoid is identified as rhodonite, on the basis of the value of $2V\gamma$ (66°). The

occurrence of tephroite as anhedral and amoeboid porphyroblasts (up to 2.5 cm across) that commonly have round inclusions (<0.1 mm in diameter) of rhodochrosite and quartz in their cores (Fig. 4b) is in accordance with the reaction:

$$\text{rhodochrosite + quartz = tephroite} + CO_2 \qquad (6).$$
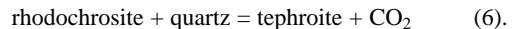
Tephroite is nearly the pure end-member, in that the iron content is below detection limits, and Mn/(Mn + Mg) ranges from 0.91 to 0.93 (Table 3). Where enclosed by rhodonite (Fig. 4c), the irregular grains of tephroite are in optical continuity and have diffuse boundaries. This feature, coupled with the identical Mn/(Mn + Mg) value (*i.e.,* within ~1–2%: Table 3) and the negligible Fe and Ca contents of the pyroxenoid (Fe, Ca < 0.05 *apfu*), suggest the replacement reaction:

$$\text{tephroite} + SiO_2 = \text{pyroxmangite} \qquad (7).$$
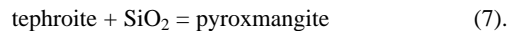
At higher temperature, pyroxmangite inverted to rhodonite *via* the well-known polymorphic transformation noted below (*e.g.,* Maresh & Mottana 1976). The silica in reaction (7) was probably introduced by fluid infiltration (see below).

Secondary carbonate and quartz in associations ii) and iii) commonly occur in irregular aggregates (0.1–1 mm across) that seem to replace rhodonite according to the reaction:

$$\text{rhodonite} + CO_2 = \text{rhodochrosite + quartz} \qquad (8).$$

The carbonates are mixtures of $MnCO_3$ and $CaCO_3$ with less than 3 mole % (Mg,Fe) components (Table 3, Fig. 5b). The Mn/Ca values are highly variable and, in

some samples (*e.g.,* Mn–4), calcite and rhodochrosite occur together.

TEM CHARACTERIZATION OF LAMELLAR DEFECTS IN RHODONITE

Most of the defects are found in pyroxmangite lamellae; they have a consistent lattice-fringe distance of 15.8 Å (*i.e.,* seven-tetrahedron chain-repeat units) and characteristically occur in groups of five (Figs. 6a, b). Other parallel defects comprise structurally disordered pyroxenoids with fringes of 29.2, 33.6 and >40 Å, which cause streaking along $c*$ (Fig. 6c); the first two are 13- and 15-tetrahedron chain-width repeats, respectively, but the last correlates with no classical pyribole. The semiquantitative compositions of the lamellae are plotted in terms of Mn/(Mn + Fe) *versus* Ca/(Ca + Mn + Fe) (Fig. 7); Mg was excluded from the plot because of its low counts:background ratio, less than 2.

In some grains, clinopyroxene defects occur as groups, or in isolation (Figs. 6a, d), alternating with pyroxmangite and disordered pyroxenoids. They exhibit neither strain contrast nor side-stepping along their length. The $(11\bar{1})$ fringe separation, 4.5 Å, parallel to the boundary [*i.e.,* $(11\bar{1})_{cpx}$ // $(001)_{rdn}$] and the nearly equally spaced $(h00)$ fringes at 106° [*i.e.,* $(h00)_{cpx}$ // $(h00)_{rdn}$] agree with typical orientations for relict lamellae of clinopyroxene in rhodonite from skarn rocks (*e.g.,* Veblen 1985, Livi & Veblen 1989, 1992). Image simulation of the experimental electron micrographs, over a range of crystal thickness and objective-lens defocus conditions (insets of Fig. 6d), enabled verification of the above relationships. Thus, at 900 Å, there is a marked similarity between simulated and observed images, and the variation in contrast with crystal thickness also is simulated. However, the experimental electron micrographs show a pattern of light spots (situated near the planes of the octahedra, over or between the octahedrally coordinated cations; *cf.* Livi & Veblen 1989), whereas the simulations show alternate rows of dark and light spots. The dark spots correlate with the (100) planes because their reflections are kinematically forbidden by the c-glide of pyroxene, whereas the light ones correspond to the (200) planes. Livi & Veblen (1989) proposed that the differences reflect dynamic scattering, which becomes significant for sufficiently thick areas and causes the odd-order $h00$ reflections to give appreciable intensities. Overall, the simulated images are consistent with lamellae of a $C2/c$ pyroxene in the orientation relationship above.

MINERALOGY OF THE SYNMETAMORPHIC VEINS

The synmetamorphic veins consist of a fine-grained (0.1–1 mm) mosaic of quartz and subordinate manganocummingtonite averaging respectively ~85 and ~15 vol.% (Fig. 4d). The nematoblasts of colorless cummingtonite ($2V\gamma$ in the range 86–88° and $c \wedge \gamma$ in the

TABLE 4. REPRESENTATIVE COMPOSITIONS OF MINERALS IN THE QUARTZ – AMPHIBOLE ± BRAUNITE VEIN OF THE VITTINKI GROUP, SOUTHWESTERN FINLAND

Locality	Kivimäki		Kivimäki				
Sample	Mn-1		Mn-3				
Mineral	cum	cum	cum	gru	act	tr	di
SiO$_2$(wt%)	57.00	54.48	54.70	51.60	54.10	55.41	51.99
TiO$_2$	<d.l.*	0.02	<d.l.	<d.l.	<d.l.	0.03	0.03
Al$_2$O$_3$	0.17	0.05	0.17	0.19	0.28	0.19	<d.l.
Cr$_2$O$_3$	<d.l.	0.00	<d.l.	<d.l.	<d.l.	<d.l.	0.04
FeO$_{tot}$	3.60	11.86	12.00	18.00	6.00	2.02	1.69
MnO	12.10	10.18	10.20	12.60	6.80	9.41	9.78
MgO	24.30	19.13	19.20	13.00	18.60	21.07	13.95
CaO	1.20	1.03	0.60	1.00	9.00	8.19	21.45
Na$_2$O	<d.l.	0.09	<d.l.	<d.l.	<d.l.	0.24	0.13
K$_2$O	<d.l.	<d.l.	<d.l.	<d.l.	<d.l.	0.12	<d.l.
F	1.60	0.92	1.10	<d.l.	0.70	0.87	<d.l.
Total	99.97	97.77	97.97	96.49	95.48	97.55	99.08
No. Ox	23	23	23	23	23	23	6
Si(atoms)	7.95	7.96	7.99	7.93	7.93	7.90	1.98
Al	0.03	0.01	0.03	0.03	0.05	0.03	0.00
Ti	0.00	0.00	0.00	0.00	0.00	0.00	0.00
Fe^{2+}	0.42	1.45	1.46	2.31	0.74	0.24	0.05
Mg	5.05	4.17	4.18	2.98	4.08	4.47	0.79
Mn	1.43	1.26	1.26	1.64	0.84	1.13	0.31
Ca	0.18	0.16	0.09	0.16	1.41	1.25	0.87
Na	0.00	0.03	0.00	0.00	0.00	0.06	0.01
K	0.00	0.00	0.00	0.00	0.00	0.02	0.00
Mn/(Ca+Mn+Fe+Mg)	0.20	0.18	0.18	0.23	0.11	0.16	0.15
Mg/(Mg+Fe^{2+})	0.92	0.74	0.74	0.56	0.84	0.95	0.94

Mineral abbreviations: cum: manganocummingtonite, gru: manganogrunerite, act: manganoan actinolite, tr: manganoan tremolite, di: diopside.
* Detection limits as in Table 1.

range 19–23°) have a preferred orientation; they are characterized by high Mg (4.06–5.05 *apfu*), such that the Mg/(Mg + Fe) value ranges from 0.56 to 0.92 (Table 4). The Mn content ranges from 1.20 to 1.41 *apfu*. The fluorine content is also high, up to 1.6 wt% in some grains. Many grains contain micrometric exsolution-lamellae of calcic amphibole that are typically parallel to (100) and $(\bar{1}01)$ (Mancini *et al.* 1998). The veins also contain sporadic grains of manganoan tremolite and diopside, with the formulas $(Ca_{1.23}Mn_{1.15} Mg_{4.51}Fe_{0.12})Si_8O_{22}(OH)_2$ and $(Ca_{0.87}Mn_{0.31}Mg_{0.79} Fe_{0.03})Si_2O_6$, respectively, and rare prismatic grains of braunite, the latter occurring at triple-point junctions between quartz and amphibole. Electron-microprobe analysis of the braunite is made difficult by concentric overgrowths of cryptomelane that simulate colloform structures and were deposited during supergene alteration by oxidizing hydrothermal solutions.

GEOCHEMISTRY OF THE MANGANESE-RICH LENSES

The bulk compositions of the manganese-rich beds are listed in Table 5 (samples Mn4–Mn6). The analyses indicate variable FeO$_{tot}$ contents, from a low 0.84 to a relatively Fe-rich 17.55 wt%. The iron-rich samples have a low Fe^{3+}/Fe^{2+} value (<0.13), which reflects the presence of abundant Fe^{2+} silicates and the generally low proportions of magnetite. The concentration of minor metals (Ni, Cu, Co, Cr and Zn) is low when compared with hydrogenous-type ferromanganese deposits in modern oceans (*e.g.,* Bonatti *et al.* 1976, Barrett *et al.* 1988), but it approximates that of submarine deposits (Fig. 8a) precipitated from buoyant hydrothermal plumes. The low terrigenous content, in terms of Al, Ti and K, and the correlation between Ba and MnO
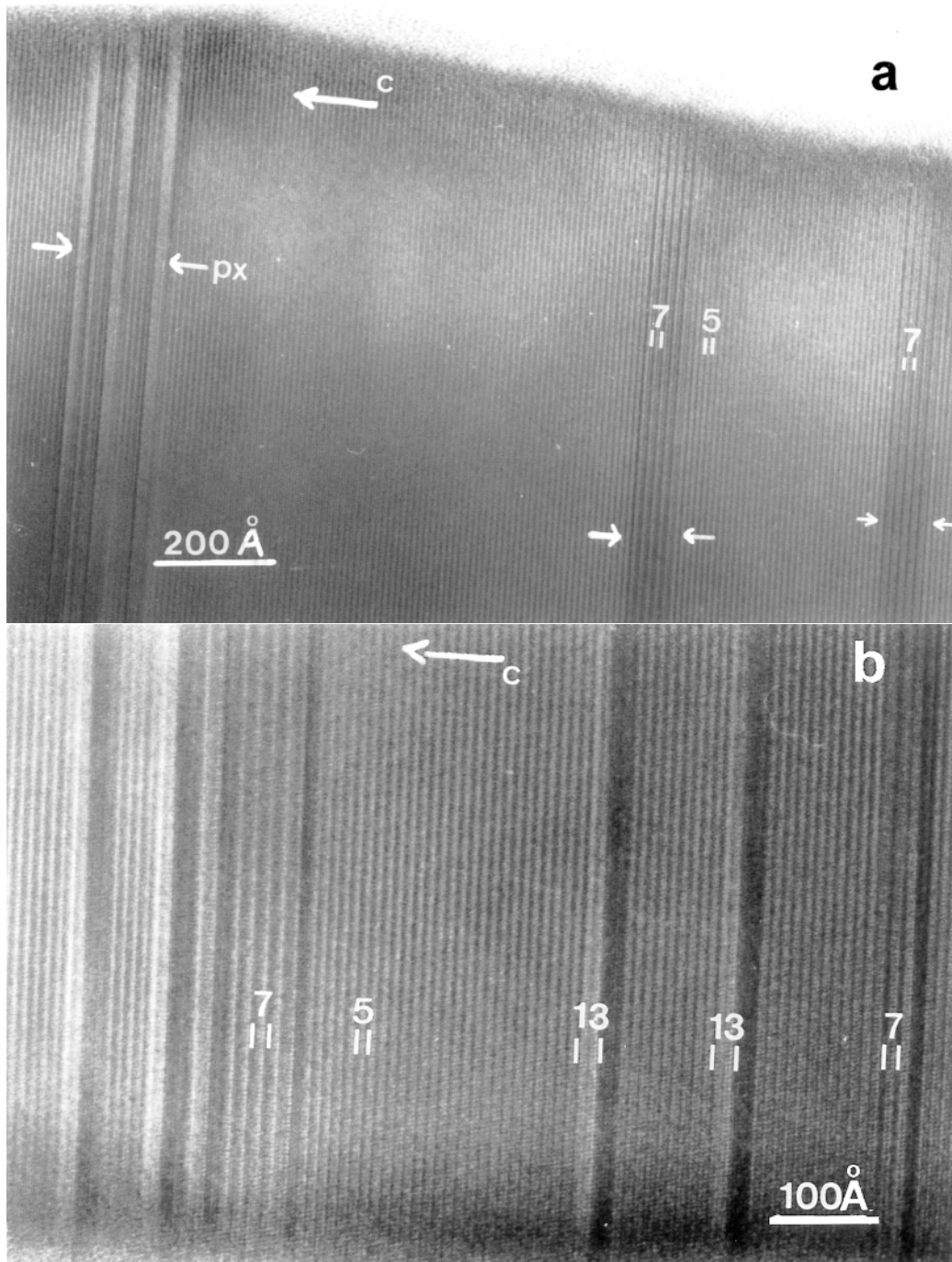
FIG. 6.   Electron micrographs of defects in rhodonite. a) and b) Pyroxmangite defects (seven-tetrahedra wide) alternating with defects having fringe spacings of 29.2 Å, which corresponds to a chain-width periodicity of 13 tetrahedra. Note the presence of pyroxene lamellae. c) Electron-diffraction pattern (SAED) of an area with pyroxmangite defects viewed down [120]. Note the spots from the pyroxmangite lattice and streaking due to disordered pyroxenoids. d) Enlarged view of the clinopyroxene defects. The inset shows the computed image; computation parameters include defocus of –900 Å and thicknesses of 50, 100, 150 and 200 Å.
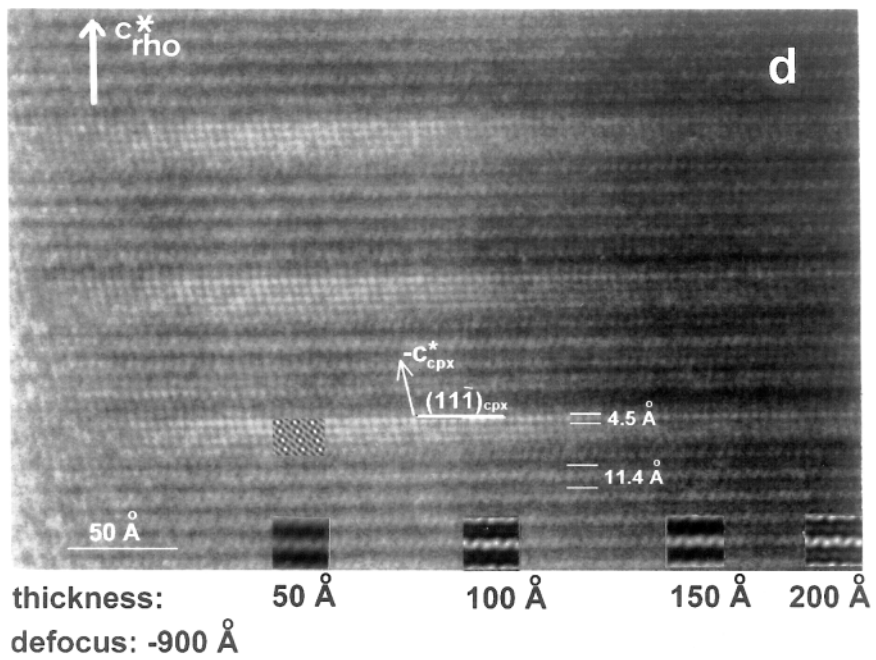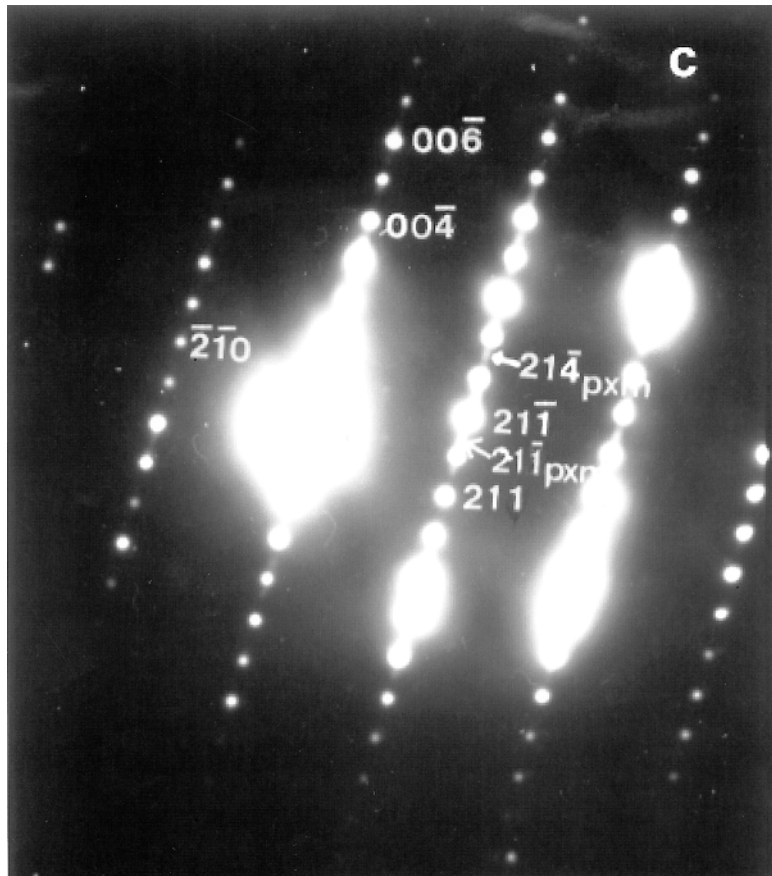
TABLE 5. REPRESENTATIVE BULK-ROCK COMPOSITIONS
OF THE MANGANESE SILICATE ROCKS
AND QUARTZ – AMPHIBOLE ± BRAUNITE VEINS
OF THE VITTINKI GROUP, SOUTHWESTERN FINLAND

*Sample	Mn-1 Kivi- mäki	Mn-2 Kivi- mäki	Mn-3 Kivi- mäki	Mn-4 Sim- psiö	Mn-5 Vitti- nki	Mn-6 Vitti- nki
SiO$_2$(wt%)	90.90	94.50	90.30	43.80	50.40	43.7
Al$_2$O$_3$	0.07	0.03	0.03	0.04	0.03	0.03
TiO$_2$	0.01	0.01	0.01	0.02	0.02	0.01
FeO	0.10	0.91	0.89	9.30	0.62	15.5
Fe$_2$O$_3$	0.67	0.18	0.18	1.37	0.24	2.28
MnO	2.59	0.91	2.35	32.40	43.80	27.90
MgO	3.58	1.71	4.45	2.81	0.76	4.10
CaO	0.22	0.08	0.30	5.44	1.29	2.93
$^{1)}$Na$_2$O	0.02	0.02	0.02	0.018	0.02	0.02
K$_2$O	0.02	0.01	0.01	<d.l.	<d.l.	<d.l.
P$_2$O$_5$	0.02	0.02	0.03	0.47	0.06	0.23
F	0.22	0.08	0.24	0.04	<d.l.	0.01
CO$_2$	0.18	0.07	0.15	1.03	0.95	0.40
H$_2$O	0.37	0.19	0.41	0.29	0.20	0.22
Total	98.96	98.71	99.36	97.02	98.38	97.32
Ba (ppm)	8	3	2	11	222	2
Co	<d.l.	5	10	8	33	3
Cr	8	11	10	<d.l.	<d.l.	<d.l.
Cu	6	18	29	<d.l.	<d.l.	<d.l.
Ni	6	5	7	<d.l.	10	<d.l.
Zn	9	11	13	68	39	10
La	0.72	0.44	0.61	1.85	0.33	2.18
Ce	0.69	0.56	0.58	2.44	0.16	2.01
Pr	0.13	0.11	0.13	0.29	<d.l.	0.36
Nd	0.57	0.37	0.62	1.28	0.31	1.45
Sm	<d.l.	<d.l.	<d.l.	0.28	<d.l.	0.36
Eu	<d.l.	<d.l.	<d.l.	0.1	0.06	0.13
Gd	0.19	<d.l.	0.15	0.30	0.29	0.83
Tb	<d.l.	<d.l.	<d.l.	0.07	<d.l.	0.17
Dy	0.17	<d.l.	0.18	0.54	0.52	1.53
Ho	<d.l.	<d.l.	<d.l.	0.15	0.17	0.44
Er	<d.l.	<d.l.	<d.l.	0.57	0.61	1.64
Tm	<d.l.	<d.l.	<d.l.	0.07	0.09	0.25
Yb	<d.l.	<d.l.	<d.l.	0.38	0.52	1.89
Mn/Si	0.04	0.01	0.04	1.22	1.44	1.06
Mn/Fe^{2+}	25.81	0.99	2.63	3.47	70.40	1.79

Detection limits (d.l.): 0.005 wt% for Si, Al, Ti, Fe, Mn, Mg, Ca,
Na and K; 0.01 wt% for F, CO$_2$ and H$_2$O; 2 ppm for Ag, Mo, Pb,
V, Y, Sr, Ni, Cu, Cr, Co, Ba and Cd; 50 ppm S and Cl; 0.10 ppm
for La, Ce, Pr, Nd, Gd, Dy, Er, Yb, 0.05 ppm for Eu, Tb, Ho, Tm.
* Samples: Mn-4, Mn-5 and Mn-6: manganese-silicate rocks;
Mn-1, Mn-2 and Mn-3: quartz-amphibole±braunite vein.

(Table 5) typify oceanic hydrothermal deposits, as also do the low concentrations and distribution of rare-earth elements (*REE*) (Fig. 8b). However, the samples have Ce-anomalies that are less strongly negative than those of typical hydrothermal deposits, perhaps reflecting precipitation from less oxidized hot brines, which retain some Ce^{3+} in solution. In addition, the light *REE* (*LREE*) are depleted and the heavy *REE*, enriched, relative to typical hydrothermal deposits; thus, because hydrothermal precipitates (*i.e.*, Fe–Mn oxyhydroxides and carbonates) preferentially scavenge the light *REE*, this depletion would reflect a relatively shorter residence-time of the *LREE* in the source hydrothermal brine (Barrett *et al.* 1988, and references therein). Representative bulk-rock compositions of the synmetamorphic

quartz–amphibole veins (Mn1–Mn3) have low iron contents (FeO$_{tot}$ <1.07 wt%), but Fe^{3+}/Fe^{2+} values ranging between 0.177 and 6.02, greater than the enclosing manganese silicate lenses. The low content of iron impeded the formation of hematite. The *REE* patterns of the veins are similar to those of the manganese silicate lenses, indicating extensive chemical equilibration of the vein fluids with the enclosing rocks (see below).

P–T CONDITIONS OF THE COUNTRY ROCKS AND VEIN ASSEMBLAGES

The metachert lacks suitable parageneses for geothermobarometry, such that banded amphibolites (metavolcanic rocks) in the country rocks must be used to constrain the temperature and pressure of metamorphism. In the vicinity of the metachert, they consist of hornblende, cummingtonite, plagioclase, quartz, ilmenite, pyrrhotite and biotite, forming an interlocking aggregate. Secondary cummingtonite either forms felted intergrowths with hornblende or replaces it. Application of the plagioclase–hornblende geothermometer (Blundy & Holland 1990) produces a clustering of temperatures at 740 ± 20°C (Table 6). Because the plagioclase and hornblende are unzoned and the plagioclase lacks evidence of unmixing, it seems likely that the geothermometer records the blocking temperature for equilibration in this system. Turning to pressure, the Na-content of hornblende in the amphibolites constitutes the most suitable geobarometer (*e.g.*, Brown 1977). The hornblende, which contains 0.43–0.48 Na *apfu* in the *M*4 site, possibly equilibrated at a pressure in the range 4.4–4.7 kbar.

The quartz–amphibole assemblages typifying the synmetamorphic veins remain stable from the greenschist to granulite facies (Klein 1973). However, the simple mineralogy, uniform grain-size, lack of retrograde recrystallization and low modal abundance of cummingtonite, a "slow diffuser" (*i.e.*, it preserves the high-temperature isotopic composition: Farquhar *et al.* 1996), lead us to favor the use of the oxygen-isotope exchange geothermometer to calculate the temperatures of equilibration. Apparent fractionation of oxygen isotopes between quartz and cummingtonite was calculated as $\Delta_{qtz–cum}$ = 17.34 – 14.49 = 2.85‰ (Table 7). If these minerals were completely equilibrated, $\Delta_{qtz–cum}$ can be converted into an equilibrium temperature using a fractionation curve estimated as $\Delta_{qtz–cum} = 0.52 \times 10^6/T^2 + 3.48 \times 10^3/T – 1.45$ (Zheng 1993) (Fig. 9). Although the chemical formula of analyzed cummingtonite includes Mn and Fe^{2+} in the *M* sites (Table 4), the O-isotopic fractionation curve for quartz and cummingtonite cannot be affected significantly by incorporation of these elements. We may therefore assume that the chemical formula of cummingtonite is approximated by the Mg end-member. Applying the fractionation equation above, the isotopic equilibrium temperature can be graphically estimated to be 665 ± 30° (1 s.d.).
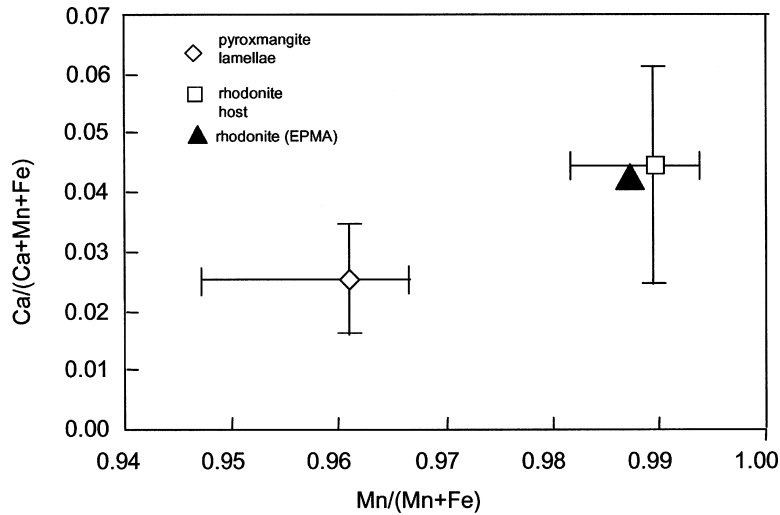
FIG. 7. Plot of Ca/(Ca + Mn + Fe) *versus* Mn/(Mn + Fe) determined by analytical electron microscopy (AEM) of host and lamellae in Mn–5. The symbols and error bars represent the mean composition and the range of values, respectively. For reference, the EPMA compositions of rhodonite are also plotted.
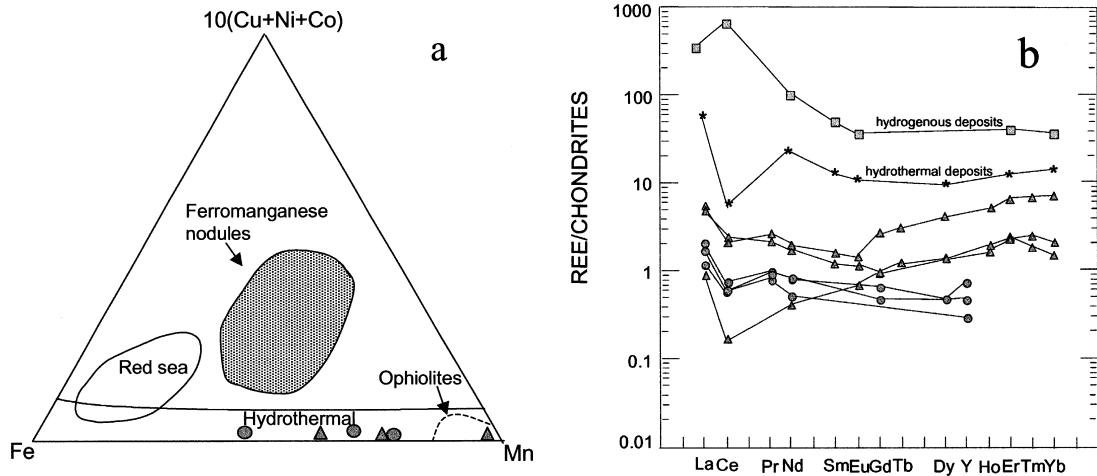

FIG. 8. a) Plot of the chemical composition of the manganese-rich rocks in terms of (Ni + Co + Cu) × 10 – Mn – Fe. b) Chondrite-normalized *REE* plot. The fields for hydrothermal and hydrogenous type deposits are from Bonatti *et al.* (1976). Symbols: manganese silicate rocks: triangles, quartz – amphibole ± braunite vein: circles.

DISCUSSION

Physicochemical conditions during metamorphism

The calculated temperature of metamorphism contrasts with that inferred from the mineral assemblages in the adjacent metapelitic schists and gneisses, over-

printed during retrograde metamorphism (Mäkitie & Lahti 1991, Niironen 1997). The high values obtained from the banded amphibolites can be ascribed to the low diffusivity of aluminum in tetrahedral coordination (Blundy & Holland 1990, Spear 1993), but the oxygen isotope temperatures from the veins are less easily explained. The temperatures, which are ~100°C above the

TABLE 6. REPRESENTATIVE COMPOSITIONS OF MINERALS OF
THE COUNTRY-ROCK AMPHIBOLITES AT VITTINKI

Locality	Vittinki			Vittinki			Vittinki			
Sample	43APH99/A			43APH99/C			43APH99/B			
Mineral	ilm	hbl	pl	hbl	pl	ilm	ilm	hbl	pl	cum
SiO_2(wt%)	<d.l.*	43.13	59.23	44.01	58.50	<d.l.	0.05	45.23	58.22	52.43
Al_2O_3	<d.l.	12.23	26.24	11.61	26.40	0.02	0.02	9.97	25.89	1.32
TiO_2	53.10	1.04	0.03	1.00	0.02	53.02	53.41	0.84	<d.l.	0.17
FeO	47.16	19.04	0.10	18.73	0.31	46.68	46.78	20.01	0.07	27.16
MgO	0.02	9.10	<d.l.	9.06	<d.l.	0.06	<d.l.	9.94	0.02	14.25
MnO	0.95	0.24	0.02	0.23	0.02	1.09	1.05	0.32	0.02	0.75
Cr_2O_3	0.02	0.06	<d.l.	<d.l.	<d.l.	<d.l.	<d.l.	0.04	0.02	<d.l.
CaO	0.03	10.65	7.65	10.70	7.75	0.05	0.06	8.72	7.84	1.22
Na_2O	<d.l.	1.71	7.33	1.51	7.52	<d.l.	<d.l.	1.21	7.19	0.15
K_2O	<d.l.	0.43	0.04	0.41	0.07	<d.l.	<d.l.	0.35	0.06	0.03
Total	101.3	97.63	100.7	97.24	100.6	100.9	101.3	96.62	99.34	97.47
No. Ox.	3	23	8	23	8	3	3	23	8	23
Si	0.00	6.50	2.627	6.63	2.61	0.00	0.00	6.85	2.62	7.86
Al	0.00	2.17	1.372	2.06	1.39	0.00	0.00	1.78	1.37	0.23
Ti	1.00	0.12	0.001	0.11	0.00	1.00	1.00	0.10	0.00	0.02
Fe^{2+}	0.98	2.40	0.004	2.36	0.01	0.98	0.97	2.53	0.00	3.40
Mg	0.00	2.05	0.001	2.03	0.00	0.00	0.00	2.24	0.00	3.18
Mn	0.02	0.03	0.001	0.03	0.00	0.02	0.02	0.04	0.00	0.10
Cr	0.00	0.01	0.000	0.00	0.00	0.00	0.00	0.00	0.00	0.00
Ca	0.00	1.72	0.364	1.73	0.37	0.00	0.00	1.41	0.38	0.20
Na	0.00	0.50	0.631	0.44	0.65	0.00	0.00	0.35	0.63	0.04
K	0.00	0.08	0.003	0.08	0.00	0.00	0.00	0.07	0.00	0.01
P=4 kbar **T°C		794.7			760.6			721.3		
P=5 kbar T°C		779.0			745.5			706.7		

Mineral abbreviations: hbl=hornblende, ilm=ilmenite, pl=plagioclase, cum=cummingtonite.
* Detection limits as in Table 1.
**calculated temperatures based on Blundy and Holland (1990).

TABLE 7. SUMMARY RESULTS OF OXYGEN ISOTOPE ANALYSES
OF MINERAL SEPARATES OF
MANGANOAN CUMMINGTONITE (Cum) AND QUARTZ (Qtz)
IN THE QUARTZ – AMPHIBOLE ± BRAUNITE VEIN

Mineral	number of samples	weight (mg)	O_2 yield (%)	$\delta^{18}O$(‰) range	$\delta^{18}O$(‰) mean	*s.d. (‰)
Cum	4	1.10-1.36	96.45-98.43	14.37-14.56	14.49	0.07
Qtz	4	0.93-1.29	91.52-95.29	17.25-17.45	17.34	0.06
$\Delta_{qtz-cum}$ (=$\delta^{18}O_{qtz}$-$\delta^{18}O_{cum}$)				2.71-2.99	2.85	0.07
**T°C				640-695	665	28

*: s.d.=standard deviation
**: calculated temperature based on the work of Zheng (1993)

closure temperatures for amphibole–quartz pairs of ~1 mm grain size (Farver & Giletti 1985), are surprisingly high, expecially considering the susceptibility of the thermometer to low-temperature re-equilibration. Perhaps the low modal amount of cummingtonite relative to quartz (*i.e.,* an "open" phase), has effectively stopped the diffusion-controlled exchange of oxygen isotopes during retrograde metamorphism(s) (see discussion in Farquhar *et al.* 1996). Conversely, the presence of abundant exsolution-induced lamellae in cummingtonite
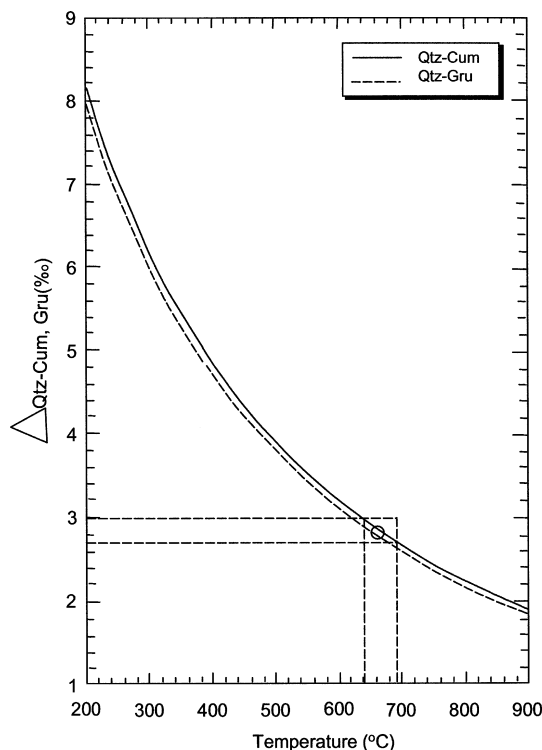
FIG. 9. Plot of the oxygen isotope fractionation between quartz and manganocummingtonite in the quartz – amphibole Å braunite vein, $\Delta_{qtz-cum}$, *versus* temperature. The fractionation curves between quartz and cummingtonite (Qtz–Cum) and quartz and grunerite (Qtz–Gru) also are plotted for comparison (see text for discussions).

(~30 vol.%, Mancini *et al.* 1998) is expected to increase the rate of diffusion (by decreasing the effective grain-size through production of new incoherent grain-boundaries; Kohn & Valley 1998), but this had no noticeable effect. A possible explanation lies in the formation of the lamellae over a large temperature-interval, say ~700–300°C (Mancini *et al.* 1998), such that only a minor proportion of the lamellae (*e.g.,* <10 vol.%) was present when the isotopic exchange stopped.

Oxygen-fugacity conditions

The oxygen fugacity determined from assemblages in the manganese silicate lenses, the metachert and the country-rock amphibolites are shown in Figure 10. Under the ambient P–T conditions, $f(O_2)$ for the country-rock amphibolites was bounded by 10^{-17} and 10^{-23} bars, respectively, as determined by the upper stability limit of ilmenite (Spear 1993) and the line of constant ilmenite composition, Ilm[99] (after Spencer & Lindsley

1981). The estimated $f(O_2)$ for the metachert was between 10^{-15} and 10^{-20} bars, as controlled by the upper stability limit of the magnetite – quartz – ferrosilite assemblage and the QFM buffer, respectively (Spear 1993). And $f(O_2)$ for the manganese silicate rocks was probably between 10^{-12} and 10^{-17} bars, on the basis of the absence of hematite and the coexistence of tephroite, quartz and magnetite (QFM buffer), respectively.

The $f(O_2)$ conditions for the quartz – amphibole ± braunite assemblages of the synmetamorphic veins with low-Fe^{2+} silicates probably were between 10^{-7} and 10^{+3} bars, on the basis of the stability field of braunite (Abs-Wurmbach *et al.* 1983). This oxidized character contrasts with the more reducing conditions determined for the manganese silicate host-rocks, yet the similar *REE*-signatures for the veins and the manganese silicate rocks suggest that the vein fluids chemically equilibrated with the latter. We suggest that the precursor vein-fluids developed in closed-system domains of the Mn-rich rocks, where $f(O_2)$ was internally buffered by mineral reactions (*e.g.,* Roy 1974). A suitable buffer is provided by the garnet-in reaction (reaction 5 above). Its steep $f(O_2)$–T gradient (Fig. 10) ensures that associated fluids become several orders of magnitude more oxidizing as peak temperatures of metamorphism are approached and attained.

Path of metamorphism of the manganese-rich assemblages

The metamorphic evolution of the manganese silicate lenses is shown schematically in Figure 11. The presence of tephroite with relict rhodochrosite and quartz inclusions is consistent with reaction (6), and is interpretable in terms of prograde metamorphism of a precursor comprising silica–carbonate mixtures. If one accepts this interpretation, it becomes possible to use the tephroite–rhodonite association [with textural evidence of earlier tephroite replacement by pyroxmangite *via* reaction (7)] to place an upper bound on $X(CO_2)$ in the prograde metamorphic fluids. We assume that the polymorphic pyroxmangite → rhodonite transformation (*i.e.,* at T approximately in the range 460–480°C at a P of 4–5 kbar: Maresh & Mottana 1976) possibly occurred isochemically (see below), because the Mn/(Mn + Fe) values of pyroxenoid and tephroite are nearly identical; the other rhodonite or pyroxmangite-rich samples have bulk Mn/Fe and Mn/Si values (1.8–70.4 and 1.06–1.44, respectively; Table 5) that overlap those needed to stabilize tephroite (*e.g.,* Dasgupta *et al.* 1993). Crystallization of pyroxmangite in preference over tephroite thus was not due to bulk composition. Similarly, the negligible Ca contents of both pyroxenoid and tephroite preclude the stabilization of pyroxmangite (over tephroite) by increased Ca activity (*e.g.,* Lucchetti 1991). And again, because $X(CO_2)$ conditions above the field of stability of tephroite (Fig. 11) require that pyroxmangite should coexist with carbonates (*e.g.,* Peters *et al.* 1973, 1977, 1978), we rule out the existence
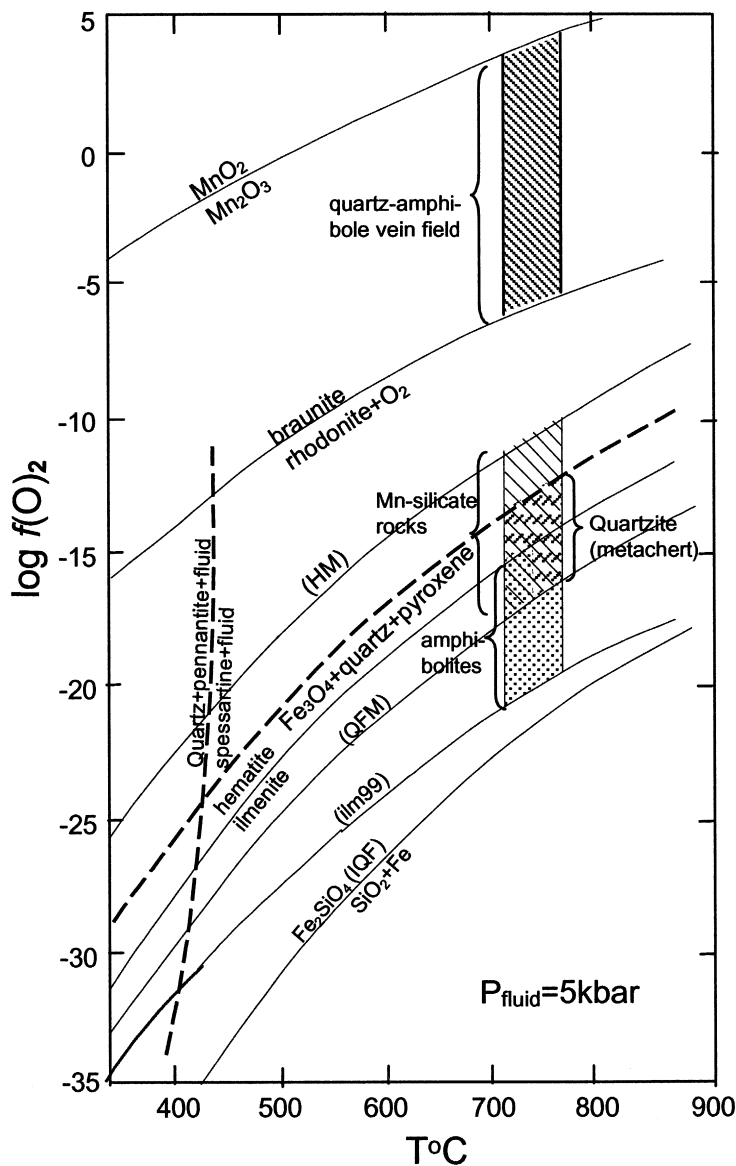
Fig. 10.   Log$f$(O_2) – T plot for various buffers of interest at P = 5 kbar. The fields for the various rocks are indicated. The buffer curves are from Spencer & Lindsley (1981), Abs-Wurmbach *et al.* (1983), and Spear (1993). The curve for reaction (5) is from Hsu (1968).

of a gradient in $X(CO_2)$ between the tephroite- and pyroxmangite-bearing associations. We therefore conclude that pyroxmangite appeared *via* the above reaction (7) under low-$X(CO_2)$ conditions [*i.e.,* $X(CO_2) \geq$ 0.02: Peters *et al.* 1973, Candia *et al.* 1975). Incomplete alteration of tephroite in association iii) is ascribed to the sluggishness of the reaction (*e.g.,* Dasgupta & Manickavasagan 1981).

Above the conditions for reaction (7), the rhodonite ± quartz association should remain stable through to the upper-amphibolite to lower-granulite facies of metamorphism. We consider that the abundant pyroxmangite-type chain defects in rhodonite in the Finnish rocks are relict structures of the lower-temperature polymorph that persisted metastably at higher temperature owing to the sluggishness of the transformation reactions (*e.g.,*
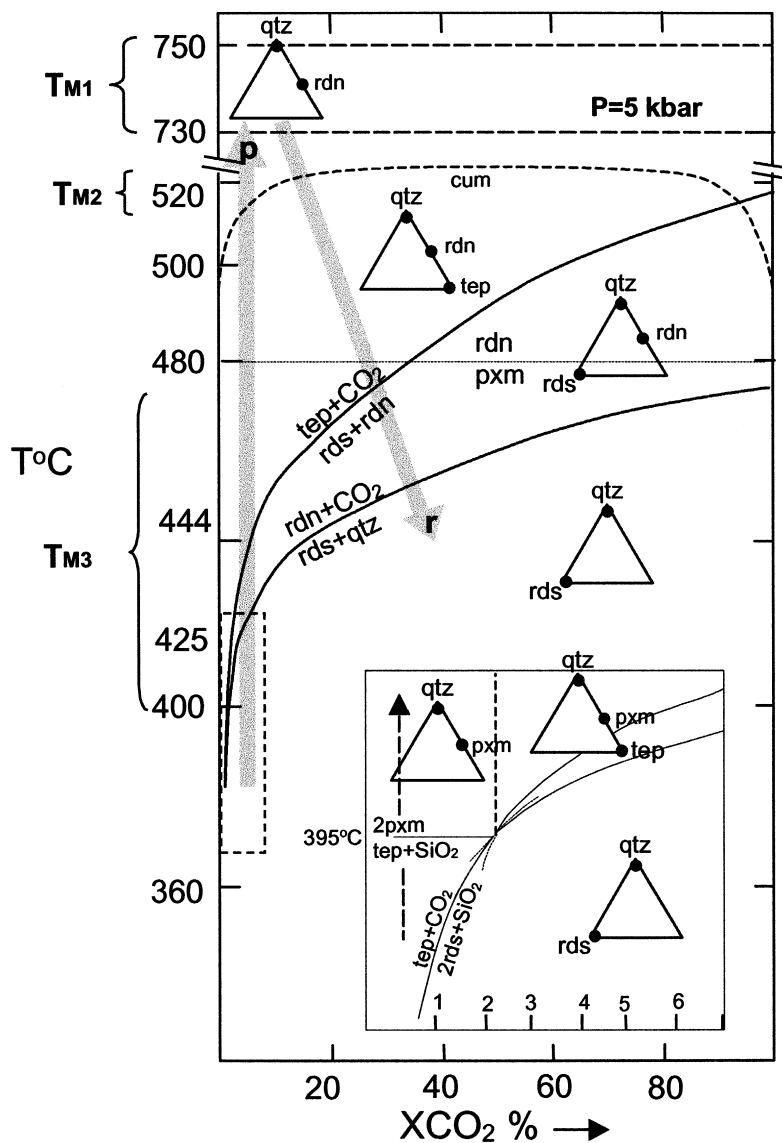
Fig. 11. Isobaric $T – X(CO_2)$ diagram for the reactions described in the text (after Peters *et al.* 1973, Candia *et al.* 1975). The paths of metamorphism for the Vittinki rocks are indicated by the arrows (p: prograde, r: retrograde). The "cum" curve indicating the upper stability limit of manganocummingtonite is from Dasgupta *et al.* (1985). The triangular diagrams show the mineral compatibilities at various temperatures. Mineral abbreviations are as in the Tables and in Figure 4.
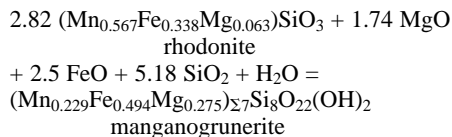
Maresh & Mottana 1976, Jefferson & Pugh 1981, Ried 1984). This interpretation is supported by the appearance, distribution and composition of the defects. Thus, unlike growth structures formed by metasomatic replacement (*e.g.,* Livi & Veblen 1992), the Ca content of the pyroxmangite lamellae overlaps with that of the host rhodonite (Fig. 7). Moreover, the (001) defects are continuous across the crystal, lack growth-induced ledges (*i.e.,* steps on the interface), and display no changes in chain type along their length. Also, the defects tend to be distributed in groups of five unit-cells, which, because every fifth fringe of pyroxmangite is coincident

with every seventh fringe of rhodonite, reduces the lattice strain at the tip. This grouping is unusual in replacement lamellae, but is common in pyroxenoids annealed at high temperature (Jefferson & Pugh 1981).

Similarly, we interpret those regions of the rhodonite crystal containing also clinopyroxene lamellae to represent an intermediate stage of the polymorphic transformation from a "protorhodonite" precursor, the clinopyroxene lamellae persisting metastably at high temperature. This is in line with the general polymorphic relationships observed in the pyroxene – pyroxenoid polysomatic series (*i.e.*, clinopyroxene → pyroxmangite → rhodonite: Ried 1984, Veblen 1985), in that the phase with a greater frequency of occurrence of horizontal offset of tetrahedra in a repeat unit of a single chain tends to occur with rising temperature (*e.g.,* Akimoto & Syono 1972, Veblen 1985), clinopyroxene having $n = \infty$, pyroxmangite, $n = 7$, and rhodonite, $n = 5$.

The cummingtonitic amphibole replacing rhodonite marks the beginning of the retrograde changes accompanying cooling. On the basis of the experimentally determined stability-curve for manganoan cummingtonite (Dasgupta *et al.* 1985), the replacement probably occurred at a temperature of approximately 550–600°C and P < 5 kbar (*i.e.,* epidote amphibolite facies). The replacement occurred under an elevated $X(H_2O)$ and at a constant, low activity of O_2, as no secondary magnetite was produced. For the mineral compositions in sample Mn–4, with $Mn/(Mn + Mg + Fe)_{cum} = 0.23$ and $Mn/(Mn + Mg + Fe)_{rdn} = 0.59$, a relevant balanced equation is:

$$2.82\ (Mn_{0.567}Fe_{0.338}Mg_{0.063})SiO_3 + 1.74\ MgO$$
$$\text{rhodonite}$$
$$+ 2.5\ FeO + 5.18\ SiO_2 + H_2O =$$
$$(Mn_{0.229}Fe_{0.494}Mg_{0.275})_{\Sigma 7}Si_8O_{22}(OH)_2$$
$$\text{manganogrunerite}$$

We assume that the amount of Mn remained constant, and that the reaction as written proceeded by consumption of Mg, Fe, SiO_2 and H_2O. The lowermost temperature for retrograde greenshist-facies metamorphism is indicated by rhodonite breakdown to carbonate + quartz (reaction 8, above). The carbonate solvus indicates a temperature range of 435–500°C for this reaction (Goldsmith & Graf 1957, Fig. 5b), whereas the experimentally determined curve suggests 400–470°C (Peters *et al.* 1973, Candia *et al.* 1975; Fig. 11).

Origin of the manganese silicate rocks

In view of the complex metamorphic history, interpretations regarding the nature of the precursor sediments must necessarily be viewed with caution. Nevertheless, the structure, mineralogy and geological association of the metacherts and manganese silicate rocks (*i.e.,* with metapelites and MORB-type metavolcanic rocks) are compatible with a submarine hydrother-

mal setting. Despite the possibility of minor metasomatism, the bulk-chemical signature of the manganese silicate lenses is akin to that from hydrothermal "post-discharge" deposits of manganese in modern oceans (Bonatti *et al.* 1976). Ni, Cu and Co sulfides are usually precipitated near the vent sites (*e.g.,* Moorby *et al.* 1984), so their near-absence from the sequence investigated possibly reflects formation from low-salinity buoyant hydrothermal plumes tens to hundreds of kilometers from the venting region (*i.e.,* ridge crest or seamounds; Fig. 12). Whether the silica-gel precursor was admixed predominantly with Mn–Fe carbonates or oxyhydroxides is difficult to assess, because both facies can yield the same metamorphic assemblages at a high temperature (Klein 1973). However, in view of the carbonate inclusions in tephroite, decarbonation of a carbonate- and silica-rich precursor is more likely, and is consistent with the derivation of alternating fayalite- and ferrosilite-rich bands in the host metachert from carbonate-rich and silica-rich layers (*e.g.,* Bonnichsen 1969). Although the low and unbuffered $X(O_2)$ allowed the carbonate to "react out", yielding Mn–Fe silicates, $X(CO_2)$ conditions were locally high (*e.g.,* the calc-silicate rocks of association iii), thereby supporting the proposal of Dasgupta *et al.* (1988) that $X(CO_2)$ can vary abruptly within a recrystallizing chert-dominated sequence.

CONCLUSIONS

1) The manganese silicate rocks found as intercalations within metachert deposit in the Bothnian Belt in southwestern Finland have lithological and compositional affinities with hydrothermal submarine deposits of Mn–Fe–Si distant from the actively venting region. They possibly formed from a precursor consisting of carbonate-rich and silica-rich layers admixed with Mn oxyhydroxides.

2) The predominance of rhodonite in the Finnish rocks results from prograde metamorphism in the presence of fluids with an unbuffered, low-$X(CO_2)$ (<0.02) fluid; the tephroite-dominant association is of local occurrence only. Peak conditions of metamorphism (T = 740 ± 30°C, P in the interval 4–5 kbar) were transitional from the upper-amphibolite to lower-granulite facies. The rhodonite contains abundant defects in chain periodicity. These defects were formed as metastable growth-related structures, suggesting that the mineral originated from a "protorhodonite" precursor through a polysomatic transformation. Synmetamorphic F2-related quartz – amphibole ± braunite veins yield temperatures of 665 ± 30°C, thereby implying that high temperatures were maintained throughout much of the episode of deformation.

3) The $f(O_2)$, at $<10^{-17}$ bars, was generally low and unbuffered during prograde metamorphism. This inference is consistent with the values for reduced and neutral assemblages in manganiferous chert (*e.g.,* Ashley
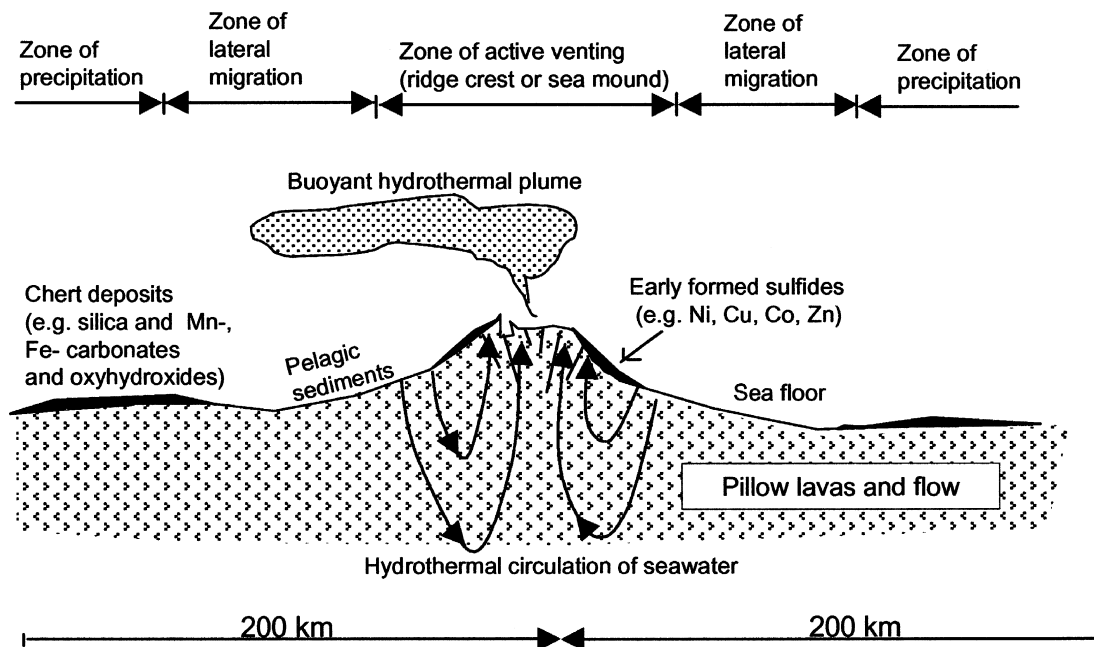
FIG. 12.   Simplified sketch showing a possible model for the formation of the precursor of the Vittinki Group rocks. Silica gel intermixed with Fe–Mn carbonates and oxyhydroxides was precipitated from a buoyant hydrothermal plume, away from the actively venting region (ridge crest or sea mounds).

1989). These predominantly reducing conditions at a high temperature explain the extensive crystallization in the Finnish rocks of the rare mineral pyroxferroite, characterized by an unusually high Fe/(Fe + Mn + Mg) value (Mancini, in prep.). The more oxidized conditions in synmetamorphic veins originated in local domains that behaved as closed systems with respect to $f(O_2)$.

REFERENCES

ABS-WURMBACH, I., PETERS, T.J., LANGER, K. & SCHREYER, W. (1983): Phase relations in the system Mn–Si–O: an experimental and petrological study. Neues Jahrb. Mineral., Abh. 146, 258-279.

AKIMOTO, S.I. & SYONO, Y. (1972): High pressure transformations in MnSiO₃. Am. Mineral. 57, 76-84.

ASHLEY, P.M. (1989): Geochemistry and mineralogy of tephroite-bearing rocks from the Hoskin manganese mine, New South Wales, Australia. Neues Jahrb. Mineral., Abh. 161, 85-111.

BARRETT, T.J., JARVIS, I., LONGSTAFFE, F.J. & FARQUHAR, R. (1988): Geochemical aspects of hydrothermal sediments in the eastern Pacific Ocean: an update. Can. Mineral. 26, 841-858.

BLUNDY, J.D. & HOLLAND, T., JR. (1990): Calcic amphibole equilibria and a new amphibole–plagioclase geothermometer. Contrib. Mineral. Petrol. 104, 208-224.

BONATTI, E., ZERBI, M., KAY, R. & RYDELL, H. (1976): Metalliferous deposits from the Appennine ophiolites: Mesozoic equivalents of modern deposits from oceanic spreading centers. Geol. Soc. Am., Bull. 87, 83-94.

BONNICHSEN, B. (1969): Metamorphic pyroxenes and amphiboles in the Biwabik iron-formation, Dunka River area, Minnesota. *Mineral. Soc. Am., Spec. Pap.* **2**, 217-239.

BROWN, E.H. (1977): The crossite content of Ca-amphibole as a guide to pressure of metamorphism. *J. Petrol.* **18**, 53-72.

BROWN, P.E., ESSENE, E.J. & PEACOR, D.R. (1980): Phase relations inferred from field data for Mn pyroxenes and pyroxenoids. *Contrib. Mineral. Petrol.* **74**, 417-425.

CANDIA, M.A.F., PETERS, T.J. & VALARELLI, J.V. (1975): The experimental investigation of the reactions $MnCO_3 + SiO_2 = MnSiO_3 + CO_2$ and $MnSiO_3 + MnCO_3 = Mn_2SiO_4 + CO_2$ in CO_2/H_2O gas mixtures at total pressure of 500 bars. *Contrib. Mineral. Petrol.* **52**, 261-266.

CLIFF, G. & LORIMER, G.W. (1975): The quantitative analysis of thin specimen. *J. Micros.* **103**, 203-207.

DASGUPTA, H.C. & MANICKAVASAGAM, R.M. (1981): Regional metamorphism of non-calcareous manganiferous sediments from India and the related petrogenetic grid for a part of the system Mn–Fe–Si–O. *J. Petrol.* **22**, 363-396.

DASGUPTA, S., BHATTACHARYA, P.K., CHATTOPADHAY, G., BANERJEE, H., MAJUMDAR, N., FUKUOKA, M. & ROY, S. (1988): Petrology of Mg–Mn amphibole bearing assemblages in manganese silicate rocks of the Sausar Group, India. *Mineral. Mag.* **52**, 105-111.

_____, MIURA, H. & HARIYA, Y. (1985): Stability of Mn-cummingtonite – an experimental study. *Mineral. J.* **12**, 251-259.

_____, SENGUPTA, P., FUKUOKA, M. & ROY, S. (1993): Contrasting parageneses in the manganese-silicate-carbonate rocks from Parseoni, Sausar Group, India and their interpretation. *Contrib. Mineral. Petrol.* **114**, 533-538.

FARQUHAR, J., CHACKO, T. & ELLIS, D.J. (1996): Preservation of oxygen isotope compositions in granulites from northwestern Canada and Enderby Land, Antarctica: implications for high-temperature isotopic thermometry. *Contrib. Mineral Petrol.* **125**, 213-224.

FARVER, J.R. & GILETTI, B.J. (1985): Oxygen diffusion in amphiboles. *Geochim. Cosmochim. Acta* **49**, 1403-1411.

GAÁL, G. & GORBATCHEV, R. (1987): An outline of the Precambrian evolution of the Baltic Shield. *Precamb. Res.* **35**, 15-52.

GOLDSMITH, J.R. & GRAF, D.L. (1957): The system CaO–MnO–CO_2: solid solution and decomposition relations. *Geochim. Cosmochim. Acta* **11**, 310-334.

HIETANEN, A. (1938): On the petrology of the Finnish quartzites. *Bull. Comm. Géol. Finlande* **21**, 1-119.

HSU, L.C. (1968): Selected phase relationships in the system Al–Mn–Fe–Si–O–H: a model for garnet equilibria. *J. Petrol.* **9**, 40-83.

HUEBNER, J.S. (1986): Nature of phases synthesized along the join $(Mg,Mn)_2Si_2O_6$. *Am. Mineral.* **71**, 111-122.

JEFFERSON, D.A. & PUGH, N.J. (1981): The ultrastructure of pyroxenoid chain silicates. III. Intersecting defects in a synthetic iron–manganese pyroxenoid. *Acta Crystallogr.* **A37**, 281-286.

KILPELÄINEN, T. (1998): Evolution and 3D modelling of structural and metamorphic patterns of the Palaeoproterozoic crust in the Tampere–Vammala area, southern Finland. *Bull. Geol. Surv. Finland* **397**.

KLEIN, C., JR. (1973): Changes in mineral assemblages with metamorphism of some banded Precambrian iron-formations. *Econ. Geol.* **68**, 1075-1088.

KOHN, M.J. & VALLEY, J.W. (1998): Oxygen isotope geochemistry of the amphiboles: isotope effects of cation substitutions in minerals. *Geochim. Cosmochim. Acta* **62**, 1947-1958.

KORSMAN, K., HÖLTTÄ, P., HAUTALA, T. & WASENIUS, P. (1984): Metamorphism as indicator of evolution and structure of the crust in eastern Finland. *Geol. Surv. Finland, Bull.* **328**.

LIVI, K.J.T. & VEBLEN, D.R. (1989): Transmission electron microscopy of interfaces and defects in intergrown pyroxenes. *Am. Mineral.* **74**, 1070-1083.

_____ & _____ (1992): An analytical electron microscopy study of pyroxene-to-pyroxenoid reactions. *Am. Mineral.* **77**, 380-390.

LUCCHETTI, G. (1991): Tephroite from the Val Graveglia metacherts (Liguria, Italy): mineral data and reactions for Mn-silicates and Mn–Ca carbonates. *Eur. J. Mineral.* **3**, 63-68.

MÄKITIE, H. & LAHTI, S.I. (1991): Pre-Quaternary rocks of the Seinäjoki map-sheet area. *Geol. Surv. Finland* (1:100.000 map).

MANCINI, F., MARUMO, K., ALVIOLA, R., KOHYAMA, N. & MARSHALL, B. (1998): Nanometer-scale structures in a Mn–Mg–Fe amphibole from Vittinki Group, western Finland. *Bull. Geol. Surv. Japan* **49**, 551-569.

MARESCH, W.V. & MOTTANA, A. (1976): The pyroxmangite–rhodonite transformation for the $MnSiO_3$ composition. *Contrib. Mineral. Petrol.* **55**, 69-79.

MOORBY, S.A., CRONAN, D.S. & GLASBY, G.P. (1984): Geochemistry of hydrothermal Mn-oxide deposits from the SW Pacific island arc. *Geochim. Cosmochim. Acta* **48**, 433-441.

NIIRONEN, M. (1997): The Svecofennian orogen: a tectonic model. *Precamb. Res.* **86**, 21-44.

PETERS, T.J., SCHWANDER, H. & TROMMSDORFF, V. (1973): Assemblages among tephroite, pyroxmangite, rhochrosite, quartz: experimental data and occurrences in the Rhetic Alps. *Contrib. Mineral. Petrol.* **42**, 325-332.

_____, TROMMSDORFF, V. & SOMMERAUER, J. (1978): Manganese-pyroxenoids and carbonates: critical phase relations in metamorphic assemblages from the Alps. *Contrib. Mineral. Petrol.* **66**, 383-388.

_____, VALARELLI, J.V., COUTINHO, J.M.V., SOMMERAUER, J. & VON RAUMER, J. (1977): The manganese deposit of Buritarama (Pará, Brazil). *Schweiz. Mineral. Petrogr. Mitt.* **57**, 313-327.

RIED, H. (1984): Intergrowth of pyroxene and pyroxenoids; chain periodicity faults in pyroxene. *Phys. Chem. Minerals* **10**, 230-235.

ROY, S. (1974): Petrology of the metamorphosed manganese-silicate rocks. *Quart. J. Geol. Mining Metall. Soc. India* **46**, 267-290.

SATOH, H. (2000): Oxygen isotope microanalysis of a large orthopyroxene clast in A-881526 diogenite. *Antarct. Meteor. Res.* **13**, 238-255.

SAXÉN, M. (1925): Om mangan-järnmalmfyndigheten I Vittinki. *Fennia* **45**, 1-41.

SHARP, Z.D. (1990): A laser based microanalytical method for the in situ determination of oxygen isotope ratios of silicates and oxides. *Geochim. Cosmochim. Acta* **54**, 1353-1357.

SPEAR, F.S. (1993): *Metamorphic Phase Equilibria and Pressure–Temperature–Time Paths*. Mineralogical Society of America, Washington, D.C.

SPENCER, K.J. & LINDSLEY, D.H. (1981): A solution model for coexisting iron–titanium oxides. *Am. Mineral.* **66**, 1189-1201.

TÖRNROOS, R. (1982): Properties of alabandite: alabandite from Finland. *Neues Jahrb. Mineral., Abh.* **144**, 107-123.

VAARMA, M. & KÄHKÖNEN, Y. (1994): Geochemistry of the Paleoproterozoic metavolcanic rocks at Evijärvi, western Finland. *In* Geochemistry of Proterozoic Supracrustal Rocks in Finland (M. Niironen & Y. Kähkönen, eds.). *Geol. Surv. Finland, Spec. Pap.* **19**, 47-59.

VEBLEN, D.R. (1985): TEM study of a pyroxene-to-pyroxenoid reaction. *Am. Mineral.* **70**, 885-901.

ZHENG, YONG-FEI (1993): Calculation of oxygen isotope fractionation in hydroxyl-bearing silicates. *Earth Planet. Sci. Lett.* **120**, 247-263.

APPENDIX: ANALYTICAL METHODS

Samples were collected from the manganese silicate lenses, the banded quartzite, the synmetamorphic veins and the country-rock amphibolites.

Mineral analysis

Mineral compositions were obtained by electron microprobe analysis (EMPA) at the Geological Survey of Japan (GSJ), using a JEOL 8800 Superprobe equipped with wavelength-dispersion detectors. Natural and synthetic minerals were used as standards. Working conditions for all elements were 15 kV, with a beam current of 1.8 nA, at a count rate of 100 s. The results are summarized in Tables 1, 2, 3, 4 and 6.

Transmission electron microscopy

Imaging of the rhodonite defects by high-resolution transmission electron microscopy (HRTEM) was undertaken at the National Institute of Industrial Health (NIIH), Tokyo, using the Hitachi 8000 TEM operating at 200 keV and an intermediate diameter (0.2 mm) objective aperture. The magnification was calibrated using the (001) d-value of a graphite standard. The ultrathin samples were prepared by ion-milling using a Gatan DuoMill at 4 keV. Analytical electron microscopy (AEM) of the lamellar defects was performed with an EDAX SiLi energy-dispersion detector mounted on a Philips CM12 instrument at 100 keV at GSJ, using an electron-beam diameter of ~100 nm. The element-concentration ratios were derived from X-ray intensities, recast according to Cliff & Lorimer (1975). The analysis of host and lamellae was repeated 15 times. The results, mean and range, are presented in graphic form.

Bulk-rock compositions

The bulk chemical analyses were done at the Geological Survey of Finland (GSF). The concentrations of most major and some trace elements were determined by X-ray fluorescence following routine procedures. TiO_2 and Na_2O contents were determined by ICP–AES (Inductively Coupled Plasma – Atomic Emission Spectrometry) on diluted samples. The selected samples were dissolved with hydrofluoric acid – perchloric acid treatment and lithium metaborate – sodium perborate fusion. The concentrations of the rare-earth elements (REE) were established on samples weighing 0.2 g by ICP–MS (Inductively Coupled Plasma – Mass Spectrometry). Total CO_2 and total H_2O were obtained by IR (infrared spectroscopy) using a LECO spectrometer. Total and divalent iron were calculated by titration with a solution of 0.05 N $KMnO_4$.

Oxygen isotope determinations

Oxygen isotopic analysis was performed on powders of coexisting minerals (quartz and cummingtonite in the synmetamorphic veins), prepared through crushing, sieving, acid-treatment and magnetic separation (>95% purity). Samples weighing ~1 mg were CO_2-laser-fluorinated under bromine pentafluoride (BrF_5) atmosphere (e.g., Sharp 1990). The extracted O_2 was converted to CO_2 using hot diamond, and the proportion of isotopes was measured with a Finnigan MAT 252 mass spectrometer at Tohoku University. The precision and accuracy of this laser-fluorination line were described in Satoh (2000). In Table 7, the resultant values of the oxygen isotope ratio $^{18}O/^{16}O$ are presented in conventional δ-notation against Vienna Standard Mean Oceanic Water (VSMOW): $\delta^{18}O = \{(^{18}O/^{16}O)_{sample}/(^{18}O/^{16}O)_{VSMOW} - 1\} \times 1000$ (‰). Each separate of quartz and cummingtonite was analyzed four times. The O_2 yields were better than 92% for quartz (as SiO_2) and 96% for manganoan cummingtonite (as per analyzed formula: Table 4), respectively. The precision of $\delta^{18}O$ was better than 0.1‰ (1 s.d. = ±0.07‰).